

## Chapter 2

# Principle of Gas Explosion Technology

Based on non-pollution low-pressure gas explosion technology, the author has successfully established a series of new gas explosion technology such as clean pulping, hemp clean degumming, preparation of humic acid, and low-activity xylo-oligosaccharide from straw and industrialization demonstration. The author broaden gas explosion technology to processing field of food, fruits, vegetables, and other natural materials and to development area of biobased chemicals, material, and energy. Gas explosion technology has been exploited as a common platform technology for biomass refining, but there is no analysis of transfer laws and action mechanism in gas explosion process based on the perspective of biomass feedstock characteristics. This chapter systematically analyzed the influence of raw material parameters, operating parameters, equipment parameters, and product parameters on gas explosion performance. The relationship between the mechanical properties of cell wall and heat and mass transfer, and momentum transfer of gas explosion process in transfer perspective were also analyzed. The relationship between maximum energy dissipation on material of the instantaneous discharge pressure stage and temperature, and moisture content were explored. Additionally, the relationship between discharge port area and material particle size based on the maximum energy dissipation was optimized. Material moisture content, particle size, and discharge area were further taken into gas explosion intensity factor  $R$ , and the meaning of gas explosion intensity was enriched. In the view of heat transfer, the energy consumption of the gas explosion process and the relationships between them were analyzed; the effect of initial moisture content, height-to-diameter ratio of gas explosion tank, loading coefficient, and temperature factors on gas explosion energy consumption was systemically observed. Based on the purpose of removing the secondary barrier in cellulose enzymatic hydrolysis, which is brought by pre-treatment process, this chapter studied the thermodynamics and kinetic rules of hemicellulose and lignin degradation, generation, and dissolution in gas explosion process.

## 2.1 The Main Parameters Affecting the Gas Explosion Process

### 2.1.1 Overview

There are several factors affecting the gas explosion process [1].

- ① Acid hydrolysis and thermal degradation. In gas explosion process, the hot steam with high pressure penetrates into the cellulosic feedstock and then the internal void of fibers. The combined effects of water vapor and heat result in acidic degradation and thermal degradation of cellulosic feedstocks. The low molecular weight substances then dissolve out, and the polymerization degree of fiber drops down.
- ② Mechanical tearing. When high-pressure steam is released, the hot steam molecules penetrate into internal void of fiber in the form of airflow speed released from closed pores. The hot steam inside or around the fiber flows out at high speed, which makes the fiber mechanical breakage to a certain extent. The fault is not only manifested as the fracture of glycosidic bonds in cellulose macromolecules and breakage of cellulose internal hydrogen bonds, but also reflected in the destruction of amorphous region and partial destruction of the crystalline regions.
- ③ Destructive effects of hydrogen. In gas explosion process, water steam penetrates into pores of fibers, and hydrogen bonds with partial hydroxyl on cellulose molecule chain were formed. At the same time, the high-temperature and high-pressure water conditions will exacerbate the destruction of hydrogen bonds inside cellulose, free new hydroxyl, and increase the intramolecular hydrogen bonds of cellulose. When intramolecular hydrogen bonds were broken, cellulose was rapidly cooled to room temperature. The supramolecular structure of cellulose was then frozen, and only a small part of the hydrogen bond was recombined. This allows solvent molecules easy go into space between the sheets and further damages the residual intramolecular hydrogen bonds and accelerates completely broken of other grain zone.
- ④ Structural rearrangement. Under the high temperature and high pressure, hydrogen bonds within cellulose molecules are destroyed to a certain extent. The mobility of cellulose chain increases which is conducive to orderly structure of cellulose. At the same time, the cellulose molecular chain is broken, so that the cellulose chain is more easily rearranged.

It is generally believed that in the process of gas explosion, hemicellulose is partly hydrolyzed and converted into monosaccharides and oligomers, while the lignin is degraded into sugars and phenolic oligomer. The acetyl hydrolyzed from hemicellulose chain would generate acetate under the high temperature, which would intensify the hydrolysis of glucosidic bond in hemicellulose and  $\beta$ -ester bond in lignin. Therefore, the bigger the intensity of pretreatment in a certain range, the

greater the degree of degradation of hemicellulose and lignin, and the fractionation effect is more obvious.

Operation conditions for gas explosion are related to raw material type, material use, and the performance of explosion tank. (1) There is a great difference of gas explosion conditions between straw and wood. (2) The requirements of plant raw material for pulping, chemical fiber, and biotransformation vary greatly. Therefore, different conditions of gas explosion can also be taken into account. For example, in order to get high yield pulp, appropriate measures are taken to prevent the cellulose degradation. From total utilization of biomass point of view, it should be at the lowest cost to obtain maximum yield of three components. (3) Considering gas explosion conditions from the engineering point of view, it is mainly the uniformity of gas cooking, namely the vapor transfer characteristics, which are highly correlated with the initial moisture content, particle size, material bulk density, and loading coefficient. (4) Performance of gas explosion tank also has influence on pretreatment effect, such as the ratio of discharge port diameter to the tank diameter, decompression velocity, shape of outlet pipe, and the volume of buffer tank. In addition, holding pressure and holding time are the main factors affecting gas explosion performance.

## ***2.1.2 Effect of Material Parameters on Gas Explosion***

### **2.1.2.1 The Structure and Composition of Raw Material**

The influence of gas explosion on component separation and supramolecular structure is closely related to the types and sources of the lignocellulose materials. For different kinds of lignocellulose materials, the chemical compositions (cellulose, hemicellulose, and lignin) are not the same. For example, the herbaceous and woody material requires different intensities of gas explosion. Even for the same kind of material, morphology, structure, and content of the cell are also different, such as the fiber cells with wall thickness and small cavity and parenchyma cells within wall and big cavity. Thus, vapor permeation and physical resistance for tearing are different, which affect the gas explosion pretreatment efficiency.

Herbal lignocellulosic materials have the following characteristics [2].

1. Structure is loose with low lignin content and high hemicellulose content; therefore, acetyl groups in hemicellulose are hydrolyzed in gas explosion process. The content of acetic acid is high, which has catalytic effect on raw materials. Herbal lignocellulosic materials are easily degraded in gas explosion process.
2. Phenolic hydroxyl group content of lignin in herbal lignocellulose is higher than that in wood materials.

According to the characteristics and properties, the wood is divided into softwood and hardwood.

Needlebush was named by its conifer leaves. At the same time, because needlebush is relatively soft, it is also called the softwood. Softwood is commonly represented by red pine, white pine, pinus, picea, basswood, poplar, etc. The cavity of softwood includes resin and tannin compounds. So softwood is often colored, elastic, and waterproof and is not easily affected by chemical reagent. It is a poor conductor of electricity, heat, and sound. The diameter of atypical cell of softwood is 30  $\mu\text{m}$ , and the thickness is 1–2  $\mu\text{m}$ . There are catheters between cells. Softwood material contains tracheid, ray cells, and ray tracheid. Tracheid is accounted for more than 90 % of material volume, which length is about 1.5–5.6 mm and width about 30–75  $\mu\text{m}$ .

Broadleaf wood is named by its broad leaves. Because broadleaf wood is hard, it is generally called the hardwood. Hardwood is commonly represented by walnut, yellow pineapple, camphor wood, catalpa wood, phoebe, willow, schimasuperba, locust, maple, teak, rosewood, red sandalwood, oak, aspen, west African rosewood, mahogany, cherry, beech, etc.

Hardwood contains libriform wood fiber, fiber tracheids and tracheid, which are both called wood fiber. Wood fiber with length of 0.7–1.7 mm, width of 20–40 m, accounts for 25–35 % of the wood volume, among which libriform wood fiber accounts for the most. Because of the tight structure, lignin content (20–24 %) is lower than softwood, and the pentosan content is high, which is generally between 21 and 24 %.

Comparison of structure and composition of hardwood, softwood, and herbage as well as their effects on gas explosion is shown in Table 2.1.

### 2.1.2.2 Particle Size and Pore Size Distribution

The best acting site for gas explosion is within cells. The cell size for different materials is not the same. So as to achieve the best effect of gas explosion, the particle size of the material should be at the cellular level. If particle size of the material is too large, it is not easy for steam permeation, the power of explosion is weakened, and tearing resistance is increased. If the particle size is too small, the steam cannot be maintained within cells, which lost the physical tearing effect and increases the energy consumption for precrushing material. It is also closely related to the gas explosion effect and the porosity of raw material. The morphology and structure of materials depend on the material porosity. High porosity is beneficial to steam or media to penetrate, which is conducive to the explosion pretreatment. It is difficult to penetrate with small porosity and the tear resistance is high in these media. It then requires more severe gas explosion conditions.

The dead cells of plant are the cavity structure and assume each cell as a mini-tank of gas explosion. In the moment of instantaneous decompression, water intracellular vaporizes, further increasing the initial pressure inside the cell. A large different pressure forms inside and outside the cell. This state is not stable and will work on the cell wall, causing cell wall tore. Therefore, in order to achieve good tear effect, ideal explosion sites are in cavity, rather than in the boundary of cells.

**Table 2.1** Structure and composition of hardwood, softwood, herbage, and their effects on gas explosion

	Hardwood		Softwood	Herbage	Gas explosion effect
Classification	Dicotyledon in angiosperm		Gymnosperm	Monocotyledon in angiosperm	
Secondary xylem	Catheter (0.2–1.3 mm), wood fiber (tracheid, fiber tracheids-bordered pit, libriform wood fiber-simple pit), wood parenchymatous cell, wood ray parenchyma cells		Tracheid (2–5 mm), no perforated wood ray cells and ray tracheid	Catheter and fiber cell	Tracheid arranged regular in softwood but scattered arranged in hardwood; thus, softwood is difficult pretreated for gas explosion. For herbage, secondary xylem is embedded in parenchymal cell, and it is easy for gas explosion
Cross-field	No		Ray cells crossed with fiber cells	No	Heat and mass transfer resistance of media is high in cross-field; thus, the pretreatment effect for softwood is bad under the same intensity as hardwood and herbage
Resin duct	No		Partly have	No	Resin duct will hinder heat and mass transfer, decreasing the gas explosion effect
Tracheal tissue	Have porous		No porous	Have	No porous imply the high penetration resistance
Fiber characteristics	Fiber length 0.7–1.7 mm, width 20–40 μm, accounted for 25–35 % of the total volume		Tracheid accounted for 90 % of the total volume, with length of 1.5–5.6 mm, width of 30–75 μm	Fiber cell with length of 1.0–2.0 mm, width of 10–20 μm	Softwood with larger length of fiber cell is hard for gas explosion (the larger the length fiber cell, the bigger the binding force with surrounding tissue)
Fiber arrangement regularity	Fiber arrangement is not regular and depends on the species		Fiber arrangement is regular, and structure is uniform	Fiber arrangement is regular, but the content of fiber cell is low	Fiber cell with highly lignification, fiber cell with high content and arranged regular is difficult for gas explosion

(continued)

Table 2.1 (continued)

	Hardwood	Softwood	Herbage	Gas explosion effect
Parenchymatous tissue	20–30 %, 2 times of softwood	7–8 %	The main structure	Softwood with low content of parenchyma cell is difficult for steam permeation and hard to break
Fiber cell wall	Partly have S3 layer	S3	S3	Possessing S3, it is hard for heat and mass transfer
Secondary wall of fiber cell	Thickness of S1 is larger than that of softwood	Degree of lignification is low, but crystalline degree is high in S1, vertical angle with fiber axis	/	/
	S2	3–10 $\mu\text{m}$ , accounted for 70–80 % of total thickness of cell wall, the angle with fiber axis is 10–40°	/	Fibrillation in pulping is to loose the microfibrer in S2, but S2 wrapped in S1 layer is hard for fibrillation
	S3	The angle with fiber axes 70–80°	/	/
Lignin	Low, 20–24 %	High	Low	Softwood with high content of lignin is hard for gas explosion
Pentosan	High, 21–24 %	Low	/	Softwood with low content of pentosan and acetyl groups is hard for gas explosion
Papermaking	Generally recognized that wood with uniform structure deep color is suitable for pulping	Density with too large or too small is both unsuited for pulping, and the appropriate density is 400–600 $\text{kg}/\text{m}^3$	/	/

(continued)

Table 2.1 (continued)

	Hardwood	Softwood	Herbage	Gas explosion effect
Air-dry density	/	0.32–0.70 g/m <sup>3</sup>	/	0.240–1.130 g/m <sup>3</sup>
Ratio of channel volume to the total volume	Moderation	Small	Large	The heat and mass transfer rate of herbal is much higher than that of wood
Lignin monomer	Syringyl, with ultraviolet absorption peak at 274–276 nm, is easily removed in alkali treatment	Guaiacyl, with ultraviolet absorption peak at 281–285 nm, is hard to remove by alkali treatment	Compared with wood, the content of phenolic hydroxyl group in herbal is the highest	In gas explosion, the chemical reaction is mainly the acid catalytic reaction. Guaiacyl, which is hard to remove by acid, would hinder the cell wall degradation
Molecular weight of lignin	High molecular weight, such as molecular weight of birch is 18,000		Low molecular weight, such as molecular weight of wheat straw is 8854	Lignin with low molecular weight is easy for dissolving out, so as to improve the accessibility of cellulose
Hemicellulose	Xylan	Glucan	Xylan with low molecular weight and low degree of polymerization	Under the acidic conditions of gas explosion, glucan in softwood is hardly degraded, and the herbal is easily degraded
Chemical bond	No ester bond	Few ester bond	A large number of ester bond	Ester bond is easily hydrolyzed and broken; thus, the herbal is easily degraded in gas explosion

Material used for gas explosion is best to reach the cell scale rather than the organization level. Because of the particle size with the organization scale, penetration resistance for steam and tear resistance are high. Once the work of steam on the material did not reach the modulus of rupture of cell wall, energy would convert into heat and sound, resulting in a waste of energy.

It can be seen in Table 2.2: (1) Thickness of fiber cell wall for *gramineae*, hardwood, and softwood progressively increases, while the cell wall thickness directly determines the resistance in gas explosion process; (2) The fiber length of *gramineae*, hardwood, and softwood is obvious, which determines the different particle size of materials before gas explosion. Taking corn straw as an example, the average fiber cell length of corn straw is 0.99 mm. If the particle size of material prepared for gas explosion is less than 0.99 mm, almost every cell is broken. There is no integrated cell wall structure to maintain the internal pressure of cell and to cause pressure rebound in the process of instantaneous decompression. In that case, steam is not likely to do volume work on the cell wall, losing the significance of physical tear. However, if the particle size of material is too large and composed of multi-cells, it would cause huge pressure rebound in instantaneous decompression, but tissue resistance and permeation resistance for steam are large, which would reduce the tearing effect. Therefore, the proper particle size directly determines the gas explosion pretreatment effect, which obeys the same law for softwood and hardwood.

Figure 2.1 shows the experimental results of gas explosion of corn straw. It can be seen that the best particle size of corn straw for gas explosion is 8 mm. At 8 mm, the degradation rate of hemicellulose and enzymatic hydrolysis rate reaches the maximum. When the particle size is less than 2 mm, the exposure rate of the carbohydrate and the specific surface area of material increases, respectively, with the particle size decreasing. The hemicellulose degradation rate and enzymatic hydrolysis yields increase with the increase of particle size, but they are still lower than that of with particle size at 8 mm. It is known that the average length of corn straw fiber cells is 1 mm [3], and the optimum size of 8 mm is larger than the single cell length. When the particle size is too large, which is beyond 15 mm, the enzymatic hydrolysis yields and hemicellulose degradation rate both decrease, indicating that the oversize of material increase the heat and mass transfer resistance and tear resistance and decrease gas explosion performance. The undersized material destructs its cell integrity, which is not conducive to holding pressure, thereby reducing the physical tear effect.

### 2.1.2.3 Initial Moisture Content and Rehydration Operation

Rehydration before gas explosion is also one of the most important factors affecting pretreatment efficiency. Rehydration operation is intended to regulate the initial moisture content and softens the fiber, which is conducive to fractionate the fiber without mechanical damage in gas explosion. At the same time, rehydration operation makes the fiber swelling to a certain extent and increase the degree of



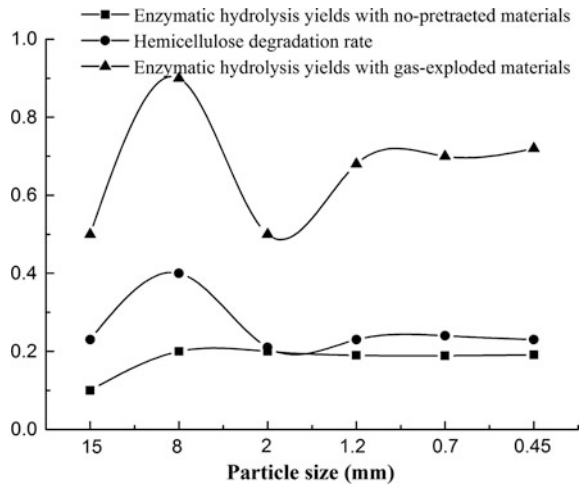
Table 2.2 Comparison of fiber morphology of common plant materials [3]

	Materials	Average length/mm	Average width/ $\mu\text{m}$	Ratio of length to width	Cell wall thickness/ $\mu\text{m}$	Cavity diameter/ $\mu\text{m}$	Ratio of cell wall to cavity	Non-fiber cell content/%
<i>Gramineae</i>	Rice straw	0.92	8.1	114	3.3	1.5	4.4	54.0
	Wheat straw	1.32	12.9	102	5.2	2.5	4.16	37.9
	Reed	1.12	9.7	115	3.0	3.4	1.77	35.5
	Silvergrass	1.36	17.1	80	6.17	3.7	3.6	34.5
	Miscan stem	1.64	16.4	100	—	—	—	53.1
	Bamboo reed	1.28	14.6	88	—	—	—	61.5
	Bagasse	1.73	22.5	77	3.28	17.9	0.36	35.7
	Chinese alpine rush	2.10	10.4	202	3.3	3.1	2.13	29.5
	Moso bamboo	2.00	16.2	123	6.6	2.90	4.55	31.2
	Sinocalamusaffinis	1.99	15.0	133	—	—	—	16.2
	Corn straw	0.99	13.2	75	—	—	—	69.2
	Sorghum stalk	1.18	12.1	109	—	—	—	51.3
	Cotton core	0.83	27.7	30	2.7	18.9	0.28	28.7
	Cotton bast	2.26	20.6	113	5.8	4.3	2.70	—

(continued)

Table 2.2 (continued)

	Materials	Average length/mm	Average width/ $\mu$ m	Ratio of length to width	Cell wall thickness/ $\mu$ m	Cavity diameter/ $\mu$ m	Ratio of cell wall to cavity	Non-fiber cell content/%
Softwood	Spruce	3.06	51.9	59	—	—	—	—
	Masson pine	3.61	50.0	72	Early wood 3.8 Late wood 8.7	Early wood 33.1 Late wood 16.6	Early wood 0.23 Late wood 1.05	1.5
	Pinus koraiensis	3.62	54.3	67	Early wood 3.5 Late wood 4.3	Early wood 27.7 Late wood 14.0	Early wood 0.25 Late wood 0.61	1.8
	Larch	3.41	44.4	77	Early wood 3.5 Late wood 9.3	Early wood 33.6 Late wood 12.6	Early wood 0.21 Late wood 1.48	1.5
	Abies nephrolepis	3.29	51.9	63	—	—	—	—
Hardwood	Poplar	0.86	17.4	50	—	—	—	23.3
	White birch	1.21	18.7	65	—	—	—	26.7
	Red birch	1.27	19.6	65	—	—	—	—
	Eucalyptus	0.68	16.8	43	—	—	—	17.6
	Batai	1.14	36.4	31	—	—	—	—

**Fig. 2.1** Particle size and its effect on gas explosion

steam penetration, so as to improve the pretreatment efficiency. In addition, the water stored in the cell cavity will be flash evaporation and volume expansion in instantaneous decompression, doing volume work on the cell wall, which is equivalent to increase the power source for physical tear. However, the bigger initial moisture content is not the better. When moisture content increase, both the energy consumption and the steam condensation will be more, which will reduce the tearing effect. So the material before gas explosion needs to be adjusted to suitable moisture content, in order to promote high-temperature cooking and physical tear.

Recovery rate of hemicellulose

$$= \frac{\text{sugar by water extract} - \text{sugar in control group}}{\text{raw material quantity} \times (1 - \text{moisture content}) \times \text{hemicellulose}} \times 100 \%$$

Loss of hemicellulose

$$= 1 - \frac{(\text{sugar by water extract} - \text{sugar in control group}) \times 0.9 + (1 - \text{water extraction rate}) \times \text{hemicellulose content in residue}}{\text{hemicellulose content in control group}} \times 100 \%$$

Figures 2.2 and 2.3 show the properties change before and after gas explosion. It can be seen that the initial moisture content of materials with 30 % before gas explosion is beneficial to the recovery rate of hemicellulose and pulp properties improved. Therefore, the appropriate initial moisture content can promote gas explosion efficiency.

Considering gas explosion conditions from engineering aspect, it is mainly the uniformity of gas transmission, which is highly correlated with the initial moisture content. The above-mentioned study shows that when the moisture content is about 34 %, both the hemicellulose recovery and cellulose hydrolysis rate are high. The initial moisture content is highly correlated with heat transfer and also may relate with hemicellulose hydrolysis kinetics and lignin softening [1].

**Fig. 2.2** Effect of the initial moisture content of materials on gas explosion effect (1.5 Mpa, 10 min) [1]

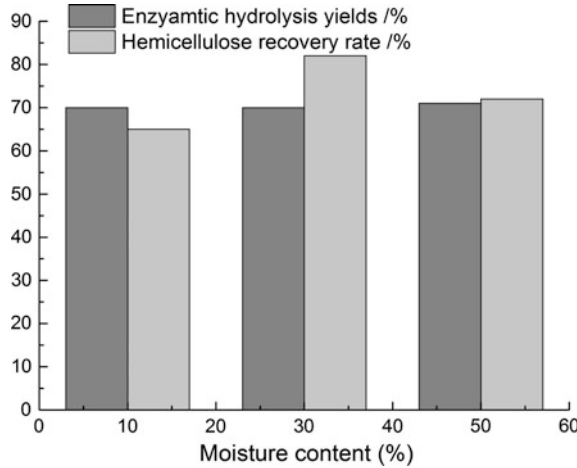
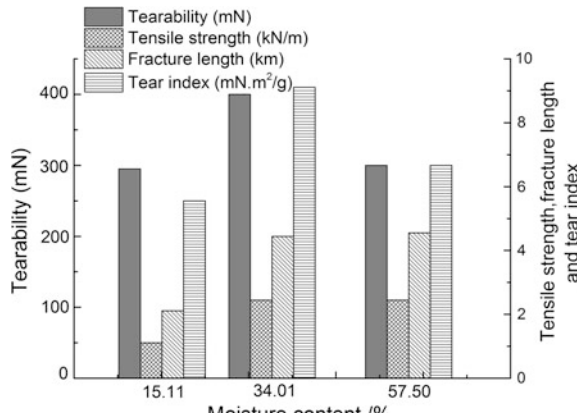


**Fig. 2.3** Effect of the initial moisture content of materials on property of pulp (1.5 Mpa, 10 min) [1]



**2.1.2.4 Loading Coefficient and Bulk Density**

The loading coefficient and bulk density affect the heat and mass transfer rate and coefficient. When bulk density is too large, the heat and mass transfer resistance increases, causing the internal and external temperatures of the material are not uniform, resulting in inhomogeneous gas explosion efficiency.

**2.1.3 Effect of Operating Parameters on Gas Explosion**

**2.1.3.1 Pre-impregnation**

Pre-impregnation has a great influence on gas explosion effect. With or without the addition of chemical reagents, the amount of added chemical reagent, soaking time,

temperature, and pressure will affect the rehydration. With or without the addition of chemical reagents, the dosage of chemical reagent, soaking time, temperature, and pressure will affect the rehydration, pH, density and hardness of materials, then has a significantly impact on steam penetration, reaction rate in high-temperature cooking, the physical tear resistance, and so on.

### **2.1.3.2 Holding Temperature**

High-temperature cooking in gas explosion process is the premise of physical tear. Besides, auto-hydrolyze effect in high-temperature cooking process leads to hemicellulose degradation and lignin softening. According to the Arrhenius equation, the temperature is increased by 10 K and the degradation rate of raw materials is increased by 2–4 times. Therefore, the effect of temperature on gas explosion effect is significant.

### **2.1.3.3 Holding Pressure**

Gas explosion process softens actually the fiber, hydrolyses the hemicellulose in high temperature, and weakens the bond between cellulose. Cellulose is torn in a sudden decompression. The pressure, namely temperature, affects the hemicellulose hydrolysis rate. At the same time, pressure is the only motivation power for physical tear. The time for holding pressure affects the degradation degree of hemicellulose and softening degree of lignin as well as the medium permeability.

### **2.1.3.4 Residence Time**

Time aims at holding pressure process. As for chemical reaction, the temperature can increase the reaction rate, but formation rate of product is related to the reaction time. Thus, the time determines the product accumulation with a certain temperature. In the process of high-temperature cooking of gas explosion, hemicellulose would be degraded into pentose, and pentose would be further converted into furfural. Lignin would be degraded into small phenolic molecules. It has been known that furfural and phenolic compounds are potential inhibitors for fermentation, so the temperature of gas explosion could not be arbitrarily increased. To obtain a certain hemicellulose degradation rate and a smaller inhibitor formation rate, reducing the temperature and prolonging the time reasonably may be a good technical measure.

### **2.1.3.5 pH Value**

The steam explosion process without the addition of acid and/or alkali is usually called autocatalytic process. Acetic acid is generated from acetyl in the cooking process, and it increases the acidity of the system. It also further promotes the

degradation of hemicellulose, which also has a catalytic role in delignification. The acid–base gas explosion means to add acid and/or alkali as the catalyst in gas explosion process. Hydrochloric acid is beneficial to the degradation of hemicellulose and improves the cellulose hydrolysis rate, and ammonia or hydrogen peroxide is beneficial for degradation and dissolution of lignin.

### ***2.1.4 Effect of Equipment Parameters on the Gas Explosion***

#### **2.1.4.1 Area of Discharge Port**

The discharge port area influences the decompression velocity. It is generally acknowledged that the bigger discharge port area the better. First of all, there is no doubt that the bigger the discharge port area is, the greater the pressure drop ( $\Delta P$  reaches the maximum and  $\Delta t$  reaches the minimum) and the bigger the superheat inside and outside cells. It illustrates that the greater the pressure rebound in material is, the larger the shock wave energy of steam acting on the cell wall, sharply tearing the cell.

#### **2.1.4.2 Shape of Outlet Pipeline**

In the process of instantaneous decompression of gas explosion, the material is transported at high speed through the pipeline to the receiver under the differential pressure of internal and external. Similar to the fluid flow in the pipeline, there is also the resistance of pipeline on transportation process of material, and the shape and structure of pipeline will cause inconsistent resistance. For example, straight pipe, bend pipe, or baffle and hammer in the inner wall of pipe all have the crushing effect on material to varying degrees. Therefore, according to the nature of material and product parameters, it should select the appropriate shape of outlet pipe.

#### **2.1.4.3 Volume of Buffer Tank**

In the first case, loading coefficient is small and the discharge port area is large enough; that is, the material can be discharged together in a very short period of time. In this case, the material does not represent a state of fluid being discharged successively, but discharged together as a group. So when the material enters into the pipeline, contacting with the barometric pressure, the pressure drop  $\Delta P/\Delta t$  can reach the maximum. Because  $\Delta P = P_1 - P_a$ ,  $\Delta t = m/\rho A u$ . In this case, the effect of buffer tank volume on gas explosion can be neglected.

In the second case, if loading coefficient is large, the discharge port area is relatively small, that is, the material is discharged in a period of time. So it can be imagined that the material discharged firstly would contact the atmospheric

pressure, and the material would then contact the pressure, which is higher than atmospheric pressure caused by the flash of the preceding material. In this case, the pressure drop rate for the discharged material is not the same; that is, to say, the work for flash gas on material is not the same, causing a different physical tear effect. This is the fundamental reason for the inhomogeneity of gas explosion.

Therefore, based on the above analysis, the volume of buffer tank (or the outlet pressure) is an important factor influencing gas explosion effect, which has an effect on the uniformity of gas-exploded materials combined with the loading coefficient and discharge port area.

### ***2.1.5 Relationship Between Product Parameters and Gas Explosion***

#### **2.1.5.1 Cell Inclusion**

Generally speaking, vegetable oils and herbal medicine components both are in the cells, and gas explosion can destroy the cell wall to increase the extraction rate of these components. For cell inclusion extraction, gas explosion is aimed at to destroy the cell wall, not need to degrade hemicellulose. Moreover, high temperature may cause decomposition of drugs and oils to reduce the content or generate the toxic substances. Therefore, in this case, low-temperature gas explosion with the media of dry air or gas–steam mixture can play the role of physical tear, reducing the damaging effects of temperature on the chemical structure.

#### **2.1.5.2 Degradation Products of Hemicellulose**

Hemicellulose accounts for about 30 % of the dry matter in lignocellulose, and the recovery rate of hemicellulose sugar in the water washing solution of gas-exploded materials can reach about 80 %. This huge resource has aroused people's concern as a platform for ethanol fermentation or acid fermentation. A lot of researches have been done on hemicellulose degradation in gas explosion process and concluded that moderately reducing the temperature and the extension time of gas explosion can increase the degradation rate and recovery rate of hemicellulose.

#### **2.1.5.3 Enzymatic Hydrolysis and Fermentation**

When lignocellulose material used as enzymatic hydrolysis and fermentation substrate, the aim of the pretreatment is to increase the exposure rate of cellulose, improve the accessibility of cellulose, and reduce the content of fermentation inhibitors.

#### **2.1.5.4 Degumming**

Similar to the hemicellulose degradation, the aim of the pretreatment in this case is to increase the degradation rate of hemicellulose but avoiding damage of the cellulose. So the pretreatment conditions could not be too intense, and moderately reducing the temperature and prolonging the time of gas explosion contribute to degumming.

#### **2.1.5.5 Pulping**

As for pulping, the aim of pretreatment of lignocellulose is mainly to remove lignin, avoiding the damage of cellulose. The lignin removal of gas explosion is limited, so alkali cooking process is generally added subsequently. Because of gas-exploded materials with hemicellulose partly removed, pores increased and material density decreased, and alkali cooking time and temperature can be reduced.

### **2.2 Multi-scale Modeling of Biomass Pretreatment for Steam Explosion Condition Optimization**

#### **2.2.1 Overview**

As it is one of the most economical and efficient biomass pretreatment technologies [4, 5], steam explosion was initially mistaken as a purely chemical process. The severity factor or modified severity factor of hydrothermal pretreatment processes is often used to describe the severity of the steam explosion process, as shown in Eqs. 2.1–2.6 in Table 2.3.

Two conclusions emerge from the effects of steam explosion on straw structure: (1) At high-temperature cooking, hemicellulose is degraded, lignin is solubilized, and cellulose binding is reduced [12]. (2) Under instantaneous decompression, superheated water flashes into steam and steam volume abruptly expands. The impact force generated by flashing and volume expansion destroys cell structure. In this stage, materials are torn into small pieces; fiber bundles are separated from one another and their structures loosen, thereby redistributing lignin; and cellulose is fully exposed.

The severity factor that currently used represents the relationship among time, temperature, and acid concentration. Although it enables the easy comparison of experimental results to facilitate process design and operation, it does not represent all the factors that affect pretreatment efficiency [9]. Unlike other hydrothermal pretreatment technologies, steam explosion is an effective fractionation technology that is characterized by physical tearing effects, which enhance lignocellulose defibration and increase specific surface area. Because the severity factor originates



**Table 2.3** Severity factor or modified severity factor in hydrothermal pretreatment processes

No.	Equations	Literature derivation
(2.1)	$R = t \cdot \exp[(T_r - T_b)/14.75]$	Overend and Chornet [6]
(2.2)	$\ln\{[Pol]/[Pol]_0\} \propto [H^+] \exp[(T_r - T_b)/14.75] \Delta t + \text{constant}$	Chum et al. [7]
(2.3)	$R_{Br}^+ = \frac{T}{T_{iso_r}} \exp\left[\frac{E_r}{ET_{iso_r}} \frac{T - T_{iso_r}}{T}\right] C_{H^+} t$ $R_{Bs}^+ = \frac{T}{T_{iso_s}} \exp\left[\frac{E_s}{ET_{iso_s}} \frac{T - T_{iso_s}}{T}\right] C_{H^+} t$	Belkacemi et al. [8]
(2.4)	$R_O = \exp\left(\frac{T - T_{ref}}{\omega}\right) \frac{t_R^{\gamma}}{\gamma}$ $R_{OH} = \exp\left(\frac{X - X_{ref}}{\lambda X_{ref}}\right) \exp\left(\frac{T - T_{ref}}{\omega}\right) \frac{t_R^{\gamma}}{\gamma}$	Abatzoglou et al. [9]
(2.5)	$R_0 = \exp\left[\frac{1}{\omega_0} \left(1 - \frac{T_{ref}}{T}\right)\right] \frac{t^{\gamma}}{\gamma}$	Montane et al. [10]
(2.6)	$R = \frac{t}{\rho_d^{1.5}} \cdot e^{\frac{T-100}{14.75}} \cdot 10^{-pH}$ $M \left( \frac{\phi D}{1 - \frac{1}{2} \pi \phi} \right)^{0.67} \left( \left( \frac{0.48 - \mu}{\mu(1-\phi)} \right)^{0.5} \left( \frac{\mu}{\phi} \right)^{0.33} \right)^{-\Delta C}$	Hosseini and Shah [11]

from hydrothermal pretreatment processes, it cannot represent the effects in the instantaneous decompression stage, but depicts those in the high-temperature cooking stage.

Hosseini and Shah [11] developed a model based on the diffusion of steam into biomass, taking particle size and process time into account (see Eq. 2.6). Although the mass transfer perspective dictates that chip size is considered first, Eq. (2.6) still represents the effects of high-temperature cooking on steam explosion. However, the equation does not depict the physical tearing effects of instantaneous decompression.

Physical tearing is affected by numerous factors such as chip size, material bulk density, material loading coefficient, and moisture content [13, 14]. The performance determinants of a pressure tank also considerably influences steam explosion results; these determinants include the height-to-diameter ratio of the tank, discharge port area [13], and buffer tank volume. Holding pressure (temperature) is another important factor.

We analyze physical tearing in instantaneous decompression on the basis of the theories of mass transfer, heat transfer, and momentum transfer as well as on brittle fracture mechanics. We consider particle size, moisture content, and discharge port area in the analysis. An enriched and comprehensive severity factor represents the effects of high-temperature cooking on steam explosion and the physical tearing effects of instantaneous decompression. Such representations enable the comprehensive interpretation of the mechanism of steam explosion technology and serve as engineering reference in designing the equipment and selecting the conditions for steam explosion technology.

## 2.2.2 Multi-scale Model Eduction in the Instantaneous Decompression Stage of Steam Explosion

### 2.2.2.1 Model Assumption

We assume that the height-to-diameter ratio of a tank is unchanged and that loading density does not affect steam transfer. The volume of a buffer tank (also called a receiver) is sufficiently large, suggesting that the environmental pressure of exported materials stabilizes at normal pressure. Hence, the variable factors are holding pressure, holding time, chip size, moisture content, and discharge port area.

Ensuring effective fractionation necessitates physical tearing at the cellular level, implying that each cell is regarded as a “micropressure tank.” A simple model for steam explosion at the cellular level is shown in Fig. 2.4.

The cell of a material is assumed to be a sphere with radius  $d$ ;  $m$  denotes the total mass of the material;  $w$  (that is,  $m_w = m \times w$ ,  $m_s = m \times (1-w)$ ) represents the moisture content;  $P_1$ ,  $T_1$ ,  $\rho_1$ , and  $m_0$  are the initial state (state 1) parameters of steam in the pressure tank;  $P_a$ ,  $T_2$ ,  $\rho_2$ , and  $m_0 + m_w$  denote the instantaneous explosion state (state 2) parameters of steam; and  $v_1$ ,  $v_2$  are the speeds of steam and solid material, respectively. The hypothetical intermediate state is easy to interpret and calculate.  $P_3$ ,  $T_2$ ,  $\rho_3$ , and  $m_0 + m_w \cdot q$  represent the intermediate state parameters of steam, and  $q$  is the vaporization ratio of heated water.

### 2.2.2.2 Establishment of a Brittle Fracture Criterion for Materials

The superheated water in cell lumens instantly flashes into steam under decompression, indicating that  $P_3 \gg P_1$ . When the brittle fracture process of materials is considered a quasi-static process, brittle fracture depends on maximal internal pressure  $P_3$ .

The stress in closed elastomers without external loads is expressed as follows:

$$\sigma_{iK} = -P\delta_{iK} \quad (2.7)$$

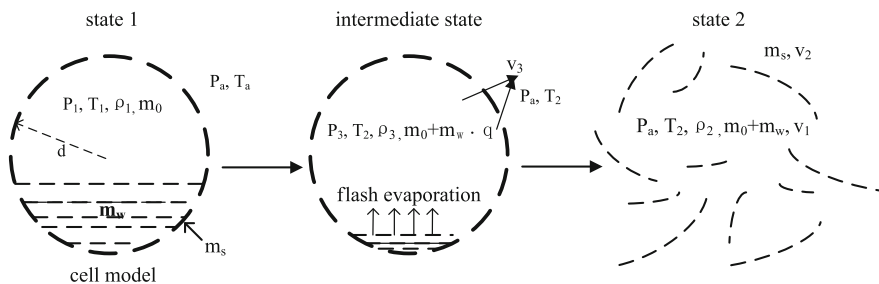


Fig. 2.4 Simple model for steam explosion at the cellular level

The elastic energy per unit mass of solid material before and after brittle fracture is written as follows [15]:

$$U_{s1} = \frac{P_3^2}{2K_s\rho_s} \quad (2.8)$$

$$U_{s2} = \frac{P_a^2}{2K_s\rho_s} \quad (2.9)$$

where  $K_s$  is the bulk modulus of solid material.

Therefore, dissipated energy  $E$  of solid material in the brittle fracture process is given as follows:

$$E = (U_{s1} - U_{s2}) \cdot m_s \quad (2.10)$$

Substituting  $U_{s1}$ ,  $U_{s2}$  from Eqs. (2.8) and (2.9) into Eq. (2.10) yields the following:

$$E = \frac{P_3^2 - P_a^2}{2 \cdot K_s \cdot \rho_s} \cdot m_s \quad (2.11)$$

In instantaneous decompression, the superheated water releases a reasonable amount of heat, thereby inducing partial vaporization into steam:

$$m_w \cdot c_m \cdot (T_1 - T_2) = m_w \cdot q \cdot r \quad (2.12)$$

where  $c_m$  is the specific heat of water, kJ/kg; and  $r$  denotes the heat of water vaporization at  $T_a$ .

According to the state equation of ideal gas,

$$P_1 V = n_1 R T_1 \quad (2.13)$$

$$P_3 V = n_2 R T_2 \quad (2.14)$$

Thus,

$$\frac{P_3}{P_1} = \frac{n_2 T_2}{n_1 T_1} = \frac{m_0 + m_w \cdot q}{m_0} \times \frac{T_2}{T_1} \quad (2.15)$$

Because

$$m_0 = \frac{MP_1 V}{RT_1} \quad (2.16)$$

Substituting Eqs. (2.12) and (2.16) into Eq. (2.15) yields the following:

$$P_3 = \left[ \frac{rMP_1V + m_w \cdot c_m(T_1 - T_2) \cdot R \cdot T_1}{rMV} \right] \times \frac{T_2}{T_1} \quad (2.17)$$

Assume

$$\frac{T_2}{T_1} \approx 0.8, P_3 = P_1 + \frac{0.2 \times m_w c_m T_1^2}{rMV} \quad (2.18)$$

Substituting  $P_3$  from Eq. (2.18) into Eq. (2.11) results in the following:

$$E = \frac{\left( P_1 + \frac{0.2 \times m_w c_m T_1^2}{rMV} \right)^2 - P_a^2}{2 \cdot K_s \cdot \rho_s} \cdot m_s \quad (2.19)$$

### 2.2.2.3 Establishment of Conservation Equations

#### 1. Energy conservation equation

The energy in the intermediate state includes internal energy  $e_1 \cdot (m_0 + m_w \cdot q)$  and potential energy  $\frac{\kappa}{\kappa-1} \cdot \frac{(m_0 + m_w) \cdot P_3}{\rho_3}$ . The energy in state 2 includes internal energy  $e_2 \cdot (m_0 + m_w \cdot q)$ , kinetic energy  $\frac{1}{2}(m_0 + m_w \cdot q)v_1^2 + \frac{1}{2}m_s v_2^2$ , and potential energy  $\frac{\kappa}{\kappa-1} \cdot \frac{(m_0 + m_w \cdot q) \cdot P_a}{\rho_2}$ .

According to the law of energy conservation,

$$\begin{aligned} & e_1(m_0 + m_w \cdot q) + \frac{\kappa}{\kappa-1} \cdot \frac{(m_0 + m_w \cdot q) \cdot P_3}{\rho_3} \\ &= e_2(m_0 + m_w) + \frac{1}{2}(m_0 + m_w \cdot q)v_1^2 + \frac{1}{2}m_s v_2^2 \\ &+ \frac{\kappa}{\kappa-1} \cdot \frac{(m_0 + m_w \cdot q) \cdot P_a}{\rho_2} + E \end{aligned} \quad (2.20)$$

where  $e_1$  and  $e_2$  are the internal energy of the unit mass of steam in the intermediate states 1 and 2, respectively, and  $\kappa$  denotes the polytropic exponent of steam [16].

The condensate state equation indicates that

$$P = A \cdot \rho^{-\kappa} \quad (2.21)$$

$$e = \frac{A}{\kappa-1} \cdot \rho^{\kappa-1} \quad (2.22)$$

where  $A$  is a constant that depends on steam.

We can determine the relationship among  $e$ ,  $P$ , and  $\rho$  as follows:

$$e = \frac{P}{\rho(\kappa - 1)} \quad (2.23)$$

Thus,

$$e_1 = \frac{P_3}{\rho_3(\kappa - 1)} \quad (2.24)$$

$$e_2 = \frac{P_a}{\rho_2(\kappa - 1)} \quad (2.25)$$

Substituting  $e$  from Eqs. (2.24) and (2.25) into Eq. (2.20) yields the following:

$$\begin{aligned} & \frac{P_3}{\rho_3(\kappa - 1)}(m_0 + m_w \cdot q) + \frac{\kappa}{\kappa - 1} \cdot \frac{(m_0 + m_w \cdot q) \cdot P_3}{\rho_3} \\ &= \frac{P_a}{\rho_2(\kappa - 1)}(m_0 + m_w \cdot q) + \frac{1}{2}(m_0 + m_w \cdot q)v_1^2 + \frac{1}{2}m_s v_2^2 \\ &+ \frac{\kappa}{\kappa - 1} \cdot \frac{(m_0 + m_w \cdot q) \cdot P_a}{\rho_2} + E \end{aligned} \quad (2.26)$$

Substituting  $E$  from Eq. (2.19) into Eq. (2.26) results in the following:

$$\begin{aligned} & \frac{P_3}{\rho_3(\kappa - 1)}(m_0 + m_w \cdot q) + \frac{\kappa}{\kappa - 1} \cdot \frac{(m_0 + m_w \cdot q) \cdot P_3}{\rho_3} \\ &= \frac{P_a}{\rho_2(\kappa - 1)}(m_0 + m_w \cdot q) + \frac{1}{2}m_s v_2^2 + \frac{1}{2}(m_0 + m_w \cdot q)v_1^2 \\ &+ \frac{\kappa}{\kappa - 1} \cdot \frac{(m_0 + m_w \cdot q) \cdot P_a}{\rho_2} + \frac{\left(P_1 + \frac{0.2 \times m_w c_m T_1^2}{rMV}\right)^2 - P_a^2}{2 \cdot K_s \cdot \rho_s} \cdot m_s \end{aligned} \quad (2.27)$$

## 2. Momentum conservation equation

The impulse that acts on solid material is equal to the increased momentum of materials in instantaneous decompression.

Because the cell of a material is assumed to be a sphere, its total stress is given as follows[17]:

$$\sigma = (P_3 - P_a)\pi d^2 \quad (2.28)$$

$$(P_3 - P_a)\pi d^2 \times t = m_s \cdot v_2 \quad (2.29)$$

where  $t$  is assumed as the decompression times, which is inversely proportional to discharge port area  $A$ .

We assume that the speed of escaping steam is constant as sound velocity [18]. Hence, the time at which steam escapes depends on the discharge port area, and  $t = \frac{\eta}{A}$ , where  $\eta$  is a coefficient that depends on the design of the discharge port. Therefore,

$$\frac{(P_3 - P_a)\pi d^2 \times \eta}{A} = m_s \cdot v_2 \quad (2.30)$$

Substituting Eq. (2.30) into Eq. (2.27) results in the following:

$$\begin{aligned} & \frac{P_3}{\rho_3(\kappa - 1)}(m_0 + m_w \cdot q) + \frac{\kappa}{\kappa - 1} \cdot \frac{(m_0 + m_w \cdot q) \cdot P_3}{\rho_3} \\ &= \frac{P_a}{\rho_2(\kappa - 1)}(m_0 + m_w \cdot q) + \frac{\left(P_1 + \frac{0.2 \times m_w \cdot c_m T_1^2}{rMV} - P_a\right)^2 \cdot \pi^2 \cdot d^4 \cdot \eta^2}{2 \cdot A^2 \cdot m_s} \\ & \quad + \frac{1}{2}(m_0 + m_w \cdot q)v_1^2 + \frac{\kappa}{\kappa - 1} \cdot \frac{(m_0 + m_w \cdot q) \cdot P_a}{\rho_2} \\ & \quad + \frac{\left(P_1 + \frac{0.2 \times m_w \cdot c_m T_1^2}{rMV}\right)^2 - P_a^2}{2 \cdot K_s \cdot \rho_s} \cdot m_s \end{aligned} \quad (2.31)$$

Substituting Eqs. (2.12), (2.16), and (2.18) into Eq. (2.31) yields the following:

$$\begin{aligned} & \frac{\left(P_1 + \frac{0.2 \times m_w \cdot c_m T_1^2}{rMV}\right)(MP_1 V r + 0.2 \times m_w \cdot c_m RT_1^2)(\kappa + 1)}{\rho_3 RT_1 r(\kappa - 1)} \\ &= \frac{P_a \cdot (MP_1 V r + 0.2 \times m_w \cdot c_m \cdot RT_1^2) \cdot (\kappa + 1)}{RT_1 r \rho_2(\kappa - 1)} + \frac{\left(P_1 + \frac{0.2 \times m_w \cdot c_m T_1^2}{rMV} - P_a\right)^2 \cdot \pi^2 \cdot d^4 \cdot \eta^2}{2 \cdot A^2 \cdot m_s} \\ & \quad + \frac{1}{2} \left[ \frac{MP_1 V r + 0.2 \times m_w \cdot c_m \cdot RT_1^2}{RT_1 r} \right] v_1^2 + \frac{\left(P_1 + \frac{0.2 \times m_w \cdot c_m T_1^2}{rMV}\right)^2 - P_a^2}{2 \cdot K_s \cdot \rho_s} \cdot m_s \end{aligned} \quad (2.32)$$

In instantaneous decompression, speed of steam  $v_1$  is equal to sound velocity. The sound velocity is expressed as follows [18]:

$$c = \sqrt{\left(\frac{\partial P_1}{\partial \rho_1}\right)_s} = \sqrt{\kappa \frac{P_3}{\rho_3}} \quad (2.33)$$

Substituting  $v_1$  from Eq. (2.33) into Eq. (2.32) results in the following:

$$\begin{aligned}
 & \frac{\left(P_1 + \frac{0.2 \times m_w c_m T_1^2}{rMV}\right) (MP_1 V r + 0.2 \times m_w c_m R T_1^2) (\kappa + 1)}{\rho_3 R T_1 r (\kappa - 1)} \\
 &= \frac{P_a \cdot (MP_1 V r + 0.2 \times m_w \cdot c_m \cdot R T_1^2) \cdot (\kappa + 1)}{R T_1 r \rho_2 (\kappa - 1)} + \frac{\left(P_1 + \frac{0.2 \times m_w c_m T_1^2}{rMV} - P_a\right)^2 \cdot \pi^2 \cdot d^4 \cdot \eta^2}{2 \cdot A^2 \cdot m_s} \\
 &+ \frac{1}{2} \frac{(MP_1 V r + 0.2 \times m_w \cdot c_m \cdot R T_1^2) \left(P_1 + \frac{0.2 \times m_w c_m T_1^2}{rMV}\right)}{R T_1 r \rho_3} + \frac{\left(P_1 + \frac{0.2 \times m_w c_m T_1^2}{rMV}\right)^2 - P_a^2}{2 \cdot K_s \cdot \rho_s} \cdot m_s
 \end{aligned} \tag{2.34}$$

### 2.2.3 Multi-scale Model Connotation

#### 2.2.3.1 Condition Optimization for Steam Explosion Pretreatment on the Basis of Maximum Dissipated Energy E of Materials

Equation (2.19) shows that moisture content and holding pressure (or temperature) are the key factors that affect physical tearing.

The Antoine equation is widely used in calculating the saturated vapor pressure of water, but it is difficult to use in converting pressure to temperature. Thus, we fit a simple unary quadratic equation to represent the relationship between pressure and temperature:

$$P = 3.6 \times 10^7 - 179876T + 224.9 T^2 (R = 0.999) \tag{2.35}$$

Therefore, Eq. (2.19) can be converted into

$$\begin{aligned}
 E &\approx \frac{\left(P_1 + \frac{0.2 \times m_w c_m T_1^2}{rMV}\right)^2}{2 \cdot K_s \cdot \rho_s} \cdot m_s \\
 &= \frac{\left(3.6 \times 10^7 - 179876T_1 + 224.9 T_1^2 + \frac{0.2 \times m \cdot w \cdot c_m T_1^2}{rMV}\right)^2 \cdot m(1 - w)}{2 \cdot K_s \cdot \rho_s}
 \end{aligned} \tag{2.36}$$

Equation (2.36) shows that

$$E = \frac{\left(3.6 \times 10^7 - 179876T_1 + 224.9 T_1^2 + \frac{0.2 \times m \cdot w \cdot c_m T_1^2}{rMV}\right)^2 \cdot m(1 - w)}{2 \cdot K_s \cdot \rho_s} \tag{2.37}$$

$$E = (A + Bw)^2 (1 - w) (0 < w < 1) \tag{2.38}$$

$$A = \frac{(3.6 \times 10^7 - 179876T_1 + 224.9 T_1^2)\sqrt{m}}{\sqrt{2} \cdot K_s \cdot \rho_s} \quad (2.39)$$

$$B = \frac{0.2 \times m \cdot c_m T_1^2 \sqrt{m}}{rMV \sqrt{2} \cdot K_s \cdot \rho_s} \quad (2.40)$$

When first derivative

$$E' = -(A + Bw)^2 + 2B(1 - w)(A + Bw) = 0 \quad (2.41)$$

$$w_{\text{opt}} = \frac{2B - A}{3B} \quad (2.42)$$

$$E_{\text{max}} = \frac{4(A + B)^3}{27B} \quad (2.43)$$

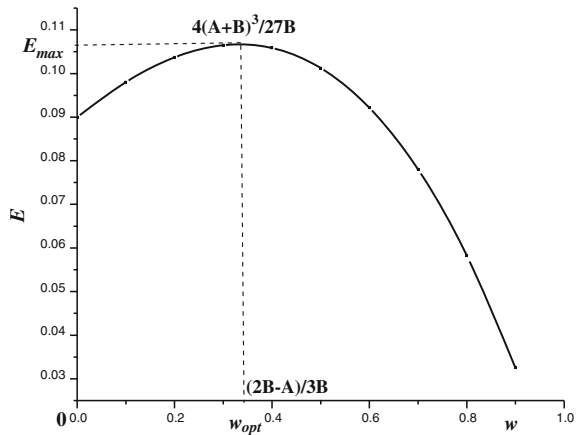
Figure 2.5 illustrates that every temperature  $T$  (range, 160–235 °C) corresponds to an optimal value for moisture content  $w_{\text{opt}}$ . In this case, dissipated energy  $E$  of solid material in the brittle fracture process reaches its maximum value. The relationship between  $T$  and  $w_{\text{opt}}$  is expressed as  $w_{\text{opt}} = \frac{2B-A}{3B}$  [ $A$  and  $B$  are shown in Eqs. (2.39) and (2.40)]. The tearing effect of solid material reaches the highest under  $T$  and  $w_{\text{opt}}$ . Hence, the effects of increased component fractionation and specific surface area also reach their best level.

As shown in Eq. (2.36),

$$E \propto T_1^4 \quad (2.44)$$

Equation (2.44) demonstrates that as temperature  $T$  increases, dissipated energy  $E$  of solid material in the brittle fracture process rises, indicating that high

**Fig. 2.5** Effect of moisture content  $w$  on dissipated energy  $E$  of materials in instantaneous decompression stage of steam explosion





temperature facilitates the tearing of solid material and the increase in specific surface area.

### 2.2.3.2 Optimizing Chip Size of Biomass and Discharge Port Area of the Steam Explosion Tank

Using the above-mentioned equations as bases, we consider holding pressure, holding time, chip size, moisture content, and discharge port area as follows:

$$\begin{aligned} & \frac{2\left(P_1 + \frac{0.2 \times m_w c_m T_1^2}{rMV} - P_a\right)(MP_1 Vr + 0.2 \times m_w c_m RT_1^2)(\kappa + 1) - (MP_1 Vr + 0.2 \times m_w \cdot c_m \cdot RT_1^2)\left(P_1 + \frac{0.2 \times m_w c_m T_1^2}{rMV}\right)(\kappa - 1)}{2\rho_3 RT_1 r(\kappa - 1)} \\ &= \frac{\left(P_1 + \frac{0.2 \times m_w c_m T_1^2}{rMV} - P_a\right)^2 \cdot \pi^2 \cdot d^4 \cdot \eta^2}{2 \cdot A^2 \cdot m_s} + \frac{\left(P_1 + \frac{0.2 \times m_w c_m T_1^2}{rMV}\right)^2 - P_a^2}{2 \cdot K_s \cdot \rho_s} \cdot m_s \end{aligned} \quad (2.45)$$

Because  $P_a \ll P_1$ , we disregard  $P_a$ . Thus,

$$\begin{aligned} & \frac{(MP_1 Vr + 0.2 \times m \cdot w \cdot c_m RT_1^2)(\kappa + 3)}{2\rho_3 RT_1 r(\kappa - 1)} \\ &= \frac{\left(P_1 + \frac{0.2 \times m \cdot w \cdot c_m T_1^2}{rMV}\right) \cdot \pi^2 \cdot d^4 \cdot \eta^2}{2 \cdot A^2 \cdot m(1 - w)} + \frac{\left(P_1 + \frac{0.2 \times m \cdot w \cdot c_m T_1^2}{rMV}\right)}{2 \cdot K_s \cdot \rho_s} \cdot m(1 - w) \end{aligned} \quad (2.46)$$

Substituting  $P_1$  from Eq. (2.35) into Eq. (2.46) results in the following:

$$\begin{aligned} & \frac{[M(3.6 \times 10^7 - 179876T_1 + 224.9 T_1^2) Vr + 0.2 \times m \cdot w \cdot c_m RT_1^2](\kappa + 3)}{2\rho_3 RT_1 r(\kappa - 1)} \\ &= \frac{\left(3.6 \times 10^7 - 179876T_1 + 224.9 T_1^2 + \frac{0.2 \times m \cdot w \cdot c_m T_1^2}{rMV}\right) \cdot \pi^2 \cdot d^4 \cdot \eta^2}{2 \cdot A^2 \cdot m(1 - w)} \\ &+ \frac{\left(3.6 \times 10^7 - 179876T_1 + 224.9 T_1^2 + \frac{0.2 \times m \cdot w \cdot c_m T_1^2}{rMV}\right)}{2 \cdot K_s \cdot \rho_s} \cdot m(1 - w) \end{aligned} \quad (2.47)$$

Equation (2.47) can be rewritten as follows:

$$K_1 T_1 + K_2 w T_1 = [K_3 T_1^2 + K_4 w T_1^2] \cdot \frac{d^4}{A^2 \cdot (1 - w)} + (K_5 T_1^2 + w K_6 T_1^2)(1 - w) \quad (2.48)$$

where

$$K_1 \approx \frac{MVr \times 224.9}{2\rho_3 Rr(\kappa - 1)} \quad (2.49)$$

$$K_2 = \frac{0.2 \times m \cdot w \cdot c_m(\kappa + 3)}{2\rho_3 r(\kappa - 1)} \quad (2.50)$$

$$K_3 \approx \frac{224.9\pi^2 \eta^2}{2m} \quad (2.51)$$

$$K_4 = \frac{0.2 \times w \cdot c_m \cdot \pi^2 \cdot \eta^2}{2rMV} \quad (2.52)$$

$$K_5 \approx \frac{224.9m}{2 \cdot K_s \cdot \rho_s} \quad (2.53)$$

$$K_6 = \frac{0.2 \times m^2 \cdot w \cdot c_m}{2 \cdot K_s \cdot \rho_s \cdot rMV} \quad (2.54)$$

Using Eq. (2.48), we derive the following:

$$T_1 = \frac{(K_1 + K_2 w)A^2 \cdot (1 - w)}{(K_3 + K_4 w) \cdot d^4 + (K_5 + wK_6)(1 - w)^2 A^2} \quad (2.55)$$

As shown in Fig. 2.2, every  $T$  corresponds to an optimal  $w_{\text{opt}}$ . Hence,  $T$  and  $w_{\text{opt}}$  can be assumed constant.

$$T = \frac{\alpha A_1^2}{\beta d_1^4 + \chi A_1^2} = \frac{\alpha A_2^2}{\beta d_2^4 + \chi A_2^2} \quad (2.56)$$

$$\alpha = (K_1 + K_2 w_{\text{opt}})(1 - w_{\text{opt}}) \quad (2.57)$$

$$\beta = K_3 + K_4 w_{\text{opt}} \quad (2.58)$$

$$\chi = (K_5 + w_{\text{opt}}K_6)(1 - w_{\text{opt}})^2 \quad (2.59)$$

Using Eq. (2.56), we derive the following:

$$\frac{A_1}{A_2} = \left( \frac{d_1}{d_2} \right)^2 \quad (2.60)$$

i.e.,

$$A \propto d^2 \quad (2.61)$$

As depicted in Eqs. (2.60) and (2.61), discharge port area  $A$  and radius  $d$  are relevant under  $T$  and  $w_{\text{opt}}$ , and the relationship between these variables is expressed as  $A \propto d^2$ . This relationship indicates that materials with different chip sizes demand different discharge port areas or that equipment with fixed discharge port areas requires corresponding chip sizes to reach the best physical tearing effect. Hence, the chip size of materials that are pretreated by steam explosion is not randomly chosen but restricted by specific equipment requirements.

### 2.2.4 Establishing a Novel Severity Factor on the Basis of Chip Size, Discharge Port Area, and Moisture Content

If severity factor  $R$  is used to describe the severity of the steam explosion process, then chemical and physical effects are incorporated into the process.

Substituting  $T_1$  from Eq. (2.55) into Eq. (2.6) yields the following:

$$R = \frac{t \cdot d^{-1.5}}{K_7} \cdot e^{\frac{(K_1 + K_2 w)A^2 \cdot (1-w)}{(K_3 + K_4 w)d^4 + (K_5 + wK_6)(1-w)^2 A^2} - 373} \cdot 10^{-\text{pH}} \quad (2.62)$$

where

$$K_7 = \frac{\rho}{M \left( \frac{\phi D}{1 - \frac{1}{2} \ln \phi} \right)^{0.67} \left( \left( 0.48 \frac{\rho u}{\mu(1-\varepsilon)} \right)^{0.5} \left( \frac{\mu}{\rho} \right)^{0.33} \right) \cdot \Delta C} \quad (2.63)$$

In Eq. (2.63),  $\rho$  is the density of the fluid;  $\mu$  denotes the dynamic viscosity of the fluid;  $u$  represents the velocity;  $\varepsilon$  is the dimensionless void fraction, which defined as the volume of void space over the total volume of packing;  $\phi$  is the void fraction;  $D$  denotes the actual diffusion coefficient;  $t$  is the pretreatment time spent in steam explosion;  $d$  represents the equivalent spherical radius of the particle;  $A$  is the discharge port area; and  $w$  is the moisture content of materials.

Equation (2.62) shows that chip size  $d$ , discharge port area  $A$ , and moisture content significantly affect severity factor  $R$ .

As illustrated in Eqs. (2.61) and (2.62),  $A \propto d^2$ . Let us assume that  $A = k'd^2$ . If  $A \neq k'd^2$ , the  $R$  value would be lower than that if  $A = k'd^2$ . If  $A = k'd^2$ , then  $R \propto d^{-1.5} \cdot e^{w^{-1}}$ . Both  $R$  values would decrease with increasing  $w$  and  $d$ . When we control the condition in  $A \propto d^2$ , a relatively small size  $d$  and a relatively low moisture content  $w$  result in a maximum  $R$ . Under these conditions, the effects of steam explosion reach their best level.

Except for traditional chemical factors, such as pretreatment time  $t$  and holding temperature  $T$ , enriched  $R$  causes physical effects. Enriched  $R$  improves the significances of the severity factor, enables the interpretation of the mechanism of steam explosion technology, and serves as theoretical guidance for further research. The enriched  $R$  serves as an engineering reference in designing the equipment and selecting the conditions for steam explosion under given treatment targets. However, this  $R$  should be further simplified and clarified. Issues such as the optimum ranges of chip size  $d$  and moisture content  $w$  for different materials, as well as the explicit relationship between  $A$  and  $d$ , necessitate additional research.

On the basis of maximum dissipated energy  $E$  of materials in the instantaneous decompression stage of steam explosion, we optimize moisture content  $w_{\text{opt}}$  with corresponding holding temperature  $T$  ( $T \leftrightarrow w_{\text{opt}}$ ) and material chip size  $d$  by discharge port area  $A$  ( $A \propto d^2$ ), which guides the selection of suitable operating temperatures and the matching of chip sizes and discharge port areas for materials with a certain moisture content. Efficient selection and matching generate the best physical tearing effects. The severity factor enriched with chip size, moisture content, and discharge port area represents the effects of high-temperature cooking on steam explosion and the physical tearing effects of instantaneous decompression. Such representations enable the comprehensive interpretation of the mechanism of steam explosion technology and guide equipment design and process parameter selection for steam explosion under a given set of materials, products, and treatment targets.

## 2.3 Mechanisms of the Physical and Chemical Coupling Effects of Gas Explosion

### 2.3.1 Overview

An effective pretreatment is required to achieve the dual purpose of enhancing the material enzymatic hydrolysis (EHY) and reducing the fermentation inhibitors at the same time. Currently, the growth of several pretreatment technologies makes it difficult to compare their advantages and disadvantages accurately. However, studies mostly focus on chemical pretreatment (e.g., dilute acid pretreatment) and several new pretreatment technologies (steam explosion (SE) and hot water pretreatment), which commonly involve the chemical reactions such as hemicellulose degradation and cellulose exposure, in order to enhance the EHY. Physical pretreatment, which is generally performed prior to chemical pretreatment, causes limited EHY improvement and high energy consumption. Thus, physical pretreatment is less likely to be used alone. Therefore, the general form of pretreatment is chemical and coupled physical–chemical.

Chemical pretreatment undeniably improves fiber exposure. However, its accompanying disadvantage of producing fermentation inhibitors of lignocellulosic

materials is one of the bottlenecks in the fermentation industry. On the other hand, physical pretreatment increases the specific surface area of the materials and prevents the generation of fermentation inhibitors, and the idea of its high energy consumption only focuses on technologies such as milling and crushing. SE is a cost-effective and a widely used method for pretreating lignocellulosic materials [4, 5]. A previous study defines SE not as a purely chemical process but a combined physical and chemical process [19]. This process couples the hydrothermal effects of chemical pretreatment with the comminution and tearing effects of physical pretreatment. At high-temperature cooking, hemicellulose is degraded, lignin is solubilized, and cellulose binding is reduced. The reduced cell wall strength of the materials resulting from these chemical reactions gave way to the idea of physical tearing at instantaneous decompression process. The physical tearing effect following the chemical action further breaks the tissues and cells to increase the surface area and porosity of the materials. These phenomena lead to the adsorption and mass transfer of materials in the EHY process. Therefore, the coupling effect of SE is greater than exclusive physical or exclusive chemical pretreatment, making SE the most economical, efficient, and widely used pretreatment technology.

The sole effects of physical pretreatment and chemical pretreatment as well as their combined effect of SE are explored and compared by analyzing the hemicellulose degradation yields, lignin degradation yields, the conversation of inhibitors, EHY, and pore size distribution of materials. This reveals the mechanisms of the effects of the main physical and chemical factors on pore size distribution and EHY of the materials as well as their respective weighting coefficient affecting the EHY of the materials. It will provide theoretical guidelines for comprehensive evaluation of the pretreatment technologies and strengthening of the EHY of the materials.

### ***2.3.2 Effects of SE on Degradation of Hemicellulose and Lignin***

Table 2.4 shows that all groups under the pressure 1.5 MPa increased along with increased SE temperature such as the reducing sugars, furfural derivatives, weak acids, and phenolic compounds found in the steam-exploded straw hydrolysates [5]. The reducing sugars, weak acids, and furfural derivatives are the degradation products of hemicellulose; thus, the degradation rate of hemicellulose increases with the increased SE temperature. The phenolic compounds are the degradation products of lignin; thus, the degradation rate of lignin increases with increased SE temperature. Weak acids, furfural derivatives, and phenolic compounds are considered as potential fermentation inhibitors. Hence, the formation rate of inhibitors also increases with increased SE temperature. At 294 K, the operating conditions are regarded as feeding 1.5 MPa pure N<sub>2</sub> at room temperature. Hence, this group is considered as the purely physical pretreatment group. At 328–471 K, the medium

**Table 2.4** Degradation of hemicellulose and lignin at the same pressure but different SE temperatures

Temperature (K; 1.5 MPa constant pressure)	Concentration (g/l; ratio of liquid to solid = 20)										
	Sugars	HMF	F	Acetic acid	Formic acid	Phenolic compounds	Degradation yield of hemicellulose (%)	Degradation yield of lignin (%)	Total inhibitors	Total degradation products	Enzymatic hydrolysis (EHY) (%)
No pretreatment	2.268	0.000	0.000	0.047	0.094	0.585	16.06	3.90	0.726	2.994	8.510
294	2.300	0.003	0.000	0.139	0.114	1.135	17.04	7.57	1.391	3.691	30.38
328	2.302	0.019	0.001	0.290	0.152	1.981	18.43	13.21	2.443	4.745	35.88
378	2.360	0.051	0.004	0.475	0.240	2.843	20.87	18.95	3.613	5.973	44.02
410	2.375	0.058	0.014	0.531	0.308	3.377	21.91	22.51	4.288	6.663	47.73
471	3.894	0.059	0.019	0.559	0.327	3.773	32.39	25.15	4.737	8.631	80.77

of SE is the gas mixture of saturated vapor and  $N_2$ ; thus, these groups are considered as physical and chemical coupling pretreatment groups under gradient temperature. Table 2.2 shows the comparison of each product formation under gradient temperature in SE pretreatment, the chemical action significantly contributed to the hemicellulose degradation yields, lignin degradation yields, the conversation of inhibitors, and EHY, whereas the physical action showed no obvious effects on the degradation products generation.

### 2.3.3 Effects of SE on Pore Distribution of Straw

Figure 2.6 shows that as the SE temperature increases, the pore volume of the straw increases, and the pore volume of the steam-exploded straw are greater than the unprocessed straw. With increased SE temperature, the volume of the cracks (400,000–100,000 nm) and macropores (100,000–10,000 nm) is gradually increased. The volume of the mesopores (10,000–100 nm) and micropores (100–5 nm) increases at 294–328 K with the increase of SE temperature, whereas at 328–471 K, their volume decreased. Figure 2.7 shows that the area of the cracks and macropores is very small and almost negligible. The total pore area, the crack area, and the micropore area are larger than the unhandled straw at 294–328 K and increases with increased SE temperature, whereas at 328–471 K, they are lesser than the unhandled straw and decreased with increased SE temperature.

At low temperatures (294–328 K), the high-temperature-cooking function of SE was unnoticeable and its physical tearing effect predominates. On this event, the high-pressure gas within the pores of each straw tore all of its pores result in increased pore volume and pore area. At high temperatures (328–471 K), the

**Fig. 2.6** Pore volume of straw at different steam explosion temperatures

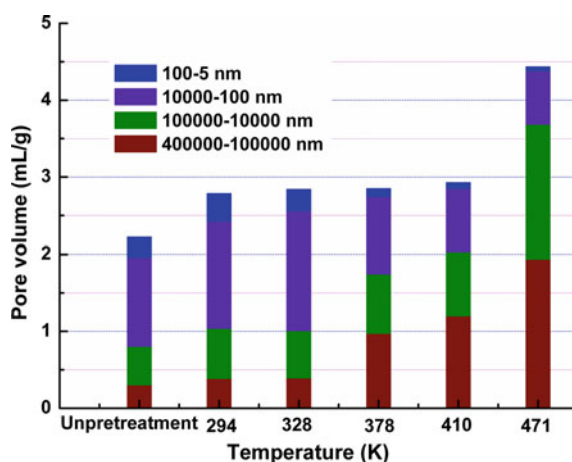
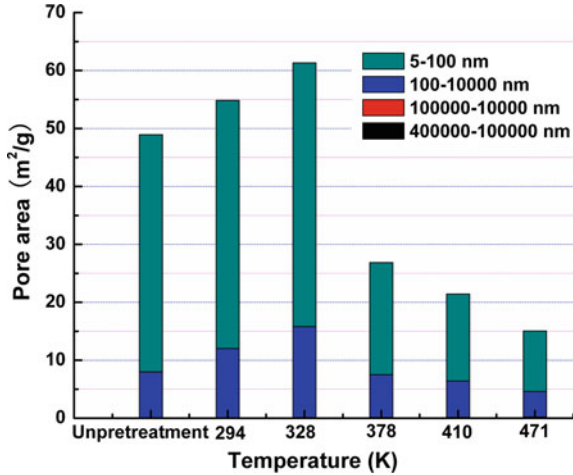


**Fig. 2.7** Pore area of straw at different steam explosion temperatures



combined chemical high-temperature cooking and physical tearing occurs. Figures 2.1 and 2.2 show that the pore volume and pore area of the mesopores and micropores sharply decreased, but the crack volume and micropores dramatically increased. Table 2.1 shows the combination of the generation of the degradation products in the steam-exploded straw wherein high-temperature cooking plays a significant role in hemicellulose and lignin degradation as well as softening and exposure of the cellulose. The cell wall consists of cellulose which acts as its skeleton, and hemicellulose and lignin as the fillers. Thus, the filler degradation caused the increase of cracks and micropores and the decrease of mesopores and micropores, then cell wall porosity was increased. The proportion of cracks and macropores in the total pore areas is less than 10 %, and that of the mesopores and micropores is more than 90 %. Thus, the strengthening role of high-temperature cooking decreases the total pore areas of the steam-exploded straw. Table 2.5 shows the influences of physical and chemical pretreatment in the pore size distribution of the steam-exploded straw. In the physical tearing process, the quantity of cracks and macropores slightly increases, whereas the mesopores and micropores noticeably increase. At low-temperature SE, the cracks and macropores account for 70 % in the total pore volumes and 10 % in the total pore areas, whereas mesopores and micropores account for 30 and 90 %, respectively, which indicated

**Table 2.5** Physical and chemical effects of SE on the pore size distribution

Content	Physical tearing effects	Chemical cooking effects	Contribution to the pore volume (%)	Contribution to the pore area (%)
Crack/macropores	Slightly increased	Increased	70	10
Macropores/micropores	Increased	Decreased	30	90



that the pore volumes and pore areas both increased based on the physical effects. In the high-temperature-cooking process, because of the increase of cracks and micropores and the decrease of mesopores and micropores, resulted in increased total pore volumes and decreased total pore areas. Therefore, the combined effects of physical tearing and chemical high-temperature cooking in SE resulted in increased pore volumes and decreased pore areas.

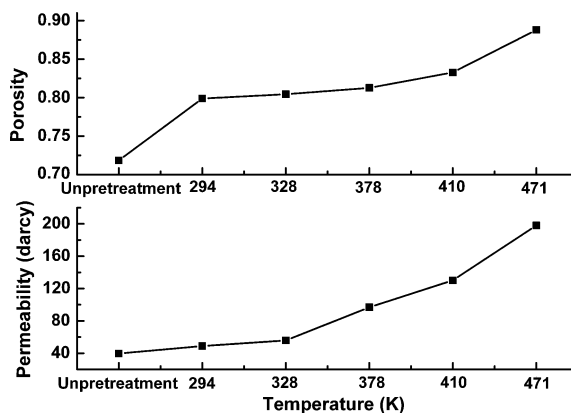
### 2.3.4 Effects of SE on Permeability of Straw

Figure 2.8 shows that compared with the un-pretreated straw, the porosity (20 %) and permeability (400 %) of the steam-exploded straw are both increased. The porosity and permeability slowly increased at low temperature (294–328 K) but significantly increased at high temperature (328–471 K), indicating that the role of high-temperature cooking in improving the porosity and permeability of materials is greater than the physical tearing. Therefore, it shows that the effects of high-temperature cooking on filler degradation within the cell wall are beneficial in opening the mesopores and micropores to improve the porosity and permeability of the materials.

### 2.3.5 Effects of SE on EHY of Straw

Table 2.6 shows that with the increase of SE pretreatment temperature, the mass fraction of the carbohydrates in the materials increases resulting from the partial degradation of lignin and hemicellulose with almost no cellulose degradation. Consequently, the relative percentage of carbohydrates including cellulose and

**Fig. 2.8** Porosity and permeability of straw at different steam explosion temperatures



**Table 2.6** Enzymatic hydrolysis of straw at different steam explosion temperature

Temperature (K; 1.5 MPa constant pressure)	Percentage of cellulose exposure (w)	EHY (%)
No pretreatment	0.70829	8.510
294	0.71627	30.38
328	0.72889	35.88
378	0.74219	44.02
410	0.75069	47.73
471	0.75713	80.77

hemicellulose increases. The increased mass fraction of carbohydrates and increased EHY in the materials are due to the exposure of a larger proportion of carbohydrates because of the degradation of lignin and hemicellulose. The content percentage of the carbohydrates is considered as the exposure proportion of carbohydrates (EPC)  $w$ , and is consistent with EHY, obtained as follows:  $\text{EHY} = 2218.8 \times \omega^{21.224}$ .

In a previous study, the effect of the pore areas (A) on EHY is calculated as follows:  $\text{EHY} = 7.40635 \times 10^{-4} \cdot A^{1.707}$ .

By comparing the two power exponents in Eqs. 2.1 and 2.2, the effects of EPC are found to be approximately 11.5 times larger than those of the pore area on the EHY of the materials, which cause the decreased material pore area and increases EHY with the increase of SE temperature. The significant increase of EPC to counter balance the negative impact of the decreased pore area on the EHY resulted in increased EHY with the increase of SE temperature.

In Table 2.3, the impact of temperature on EHY can also be measured as follows:

$$\text{EHY} = 2.15827 \cdot T^{2.2792}.$$

The impact of temperature on EHY is 1.707 compared with the lesser impact of pressure. This shows an inconsistent contribution of temperature and pressure to EHY with greater temperature effects than pressure effects. In general, for saturated steam SE, the pressure corresponds to the temperature. Hence, the strength formula of SE is  $R_0 = t \cdot \exp^{T-100/14.75}$ , where  $T$  and  $P$  refer to one parameter. However, in the present study,  $T$  and  $P$  cannot be mixed because of their different contributions to EHY. SE is a process of combined physical and chemical action that includes not only high-temperature cooking but also physical tearing, and the strength formula for SE should simultaneously contain  $T$  and  $P$ .

In SE pretreatment, chemical action significantly contributed to hemicellulose degradation yields, lignin degradation yields, the conversion of the inhibitors, and EHY, whereas physical action showed no obvious effects on the degradation products generation.

The cracks and macropores account for 70 % of the total pore volumes and 10 % of the total pore areas, whereas mesopores and micropores account for 30 and 90 %, respectively. The quantity of all pores increases in the physical tearing process, whereas the mesopores and micropores are decreased and cracks and micropores are increased in the high-temperature-cooking process. Hence, both the pore volumes and the areas increase in low-temperature SE based on the physical effects, whereas the total pore volumes increase and the total pore areas decrease in high-temperature-cooking process. Therefore, in the process of SE, the combined effects of physical tearing and chemical high-temperature cooking along with the increase of SE temperature resulted in increased pore volume and decreased pore area. With the increase of SE temperature, the pore area of the materials decreases. However, the EHY increased due to the increased EPC that is approximately 11.5 times larger than that of the pore area on EHY of materials.

## **2.4 Dissolution Thermodynamics of the Degradation Products of Steam-Exploded Straw**

### **2.4.1 Overview**

By pretreatment, lignocellulosic materials can destroy cell wall structures and increase the surface area of microfibrils [20]. However, a certain amount of xylan remains in the raw materials. Xylan covers the surface of a microfibril and forms hydrogen bonds, thus reducing the accessibility of cellulose to enzymes [21]. The US National Renewable Energy Laboratory (NREL, USA) analyzed the chemical composition of corn stover after different pretreatments. The results showed that 3.0–28.5 % of xylan remains in the substrates [22]. The affinity between xylan and cellulose resulted in the irreversible adsorption of xylan on the cellulose surface. The adsorption and dissolution of xylan are affected by environmental conditions such as temperature, substrate concentration, pH value, and ionic strength [23]. In addition, xylan accounts for about 20–30 % of the raw materials and 30 % of hydrolysates, and pentose fermentation is the key factor in determining the economical and efficient biotransformation of biomass resources [24, 25]. Thus, desorption and dissolution of xylose affect cellulose hydrolysis as well as its own conversion and utilization.

Steam explosion is used to enhance the enzymatic hydrolysis of lignocellulosic substrates into glucose and to produce hemicellulose hydrolysates with the highest yields of pentosan, which is a substrate for industrial fermentation. However, weak acids, furfural derivatives, and phenolic compounds in steam explosion hydrolysates are regarded as potential fermentation inhibitors [1] that should be removed to reduce inhibition to strains before fermentation. Therefore, the separation of oligosaccharides and potential fermentation inhibitors through dissolution eliminates the detoxification process for the fermentation industry and provides a reference for

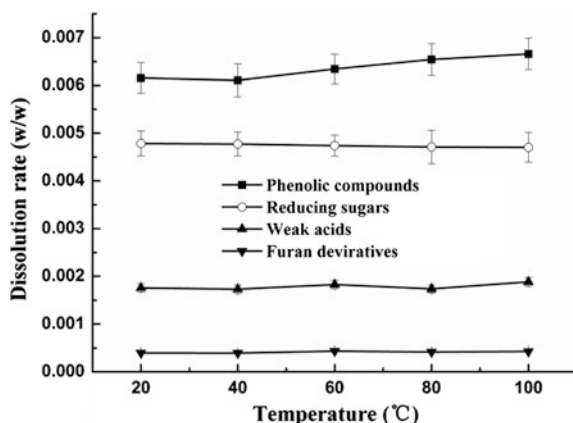
the recovery of oligosaccharides, which is beneficial to their subsequent self-conversion and utilization.

The effectiveness of oligosaccharides and fermentation inhibitors is related to their contents and energy levels. In particular, the energy state of oligosaccharides is a limiting factor to its utilization in the dissolution of degradation products during pretreatment and enzymatic hydrolysis. The energy states and the dissolution law of degradation products originating from steam-exploded straw (SES) are explored. By controlling the extraction conditions such as temperature, ionic strength, liquid-to-solid ratio (LSR) and pH, the energy states of the degradation products can be adjusted, in an attempt to realize the maximum dissolution of oligosaccharides and the minimum dissolution of potential fermentation inhibitors or hinder the dissolution of fermentation inhibitors to some extent. We aim to separate oligosaccharides and inhibitors by the dissolution process, eliminating the need for subsequent detoxification in the fermentation industry and simultaneously provide theoretical reference for the efficient dissolution and recovery of oligosaccharides.

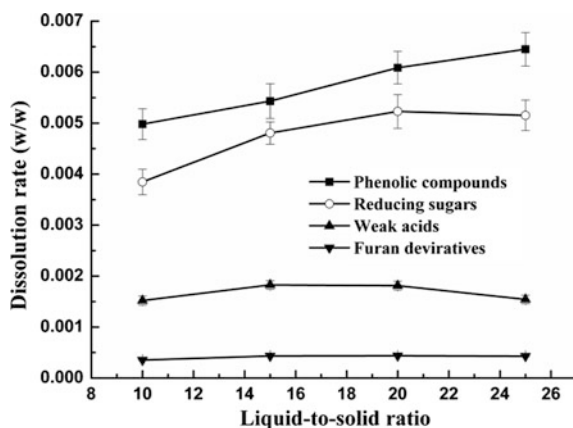
#### 2.4.2 Effects of Temperature on the Dissolution Rate of Degradation Products

As shown in Fig. 2.9, the effects of temperature on the dissolution of phenolic compounds are significant. However, temperature has little effect on the dissolution of sugars, weak acids, and furfural derivatives. With the increase of temperature, the dissolved amount of phenolic compounds also increases, whereas the dissolved amount of sugars slightly decreases. This result shows that increased temperature favors the dissolution of phenolic substances but not the dissolution of sugars.

**Fig. 2.9** Dissolution rate of degradation products of steam-exploded straw at different temperatures



**Fig. 2.10** Dissolution rate of degradation products of steam-exploded straw at different liquid-to-solid ratios



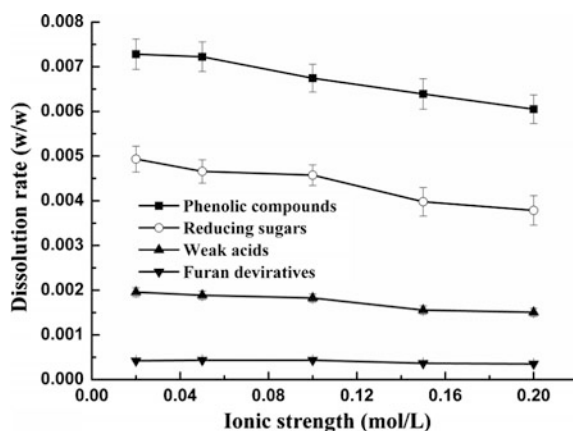
### 2.4.3 Effects of LSR on the Dissolution Rate of Degradation Products

Figure 2.10 shows that the dissolved amount of phenolic compounds and sugars increases with increased LSR. The dissolution amount of sugars can reach its maximum at LSR = 20. The dissolution of weak acids also reaches its maximum at LSR = 20. LSR almost has no effect on the dissolution of furfural derivatives.

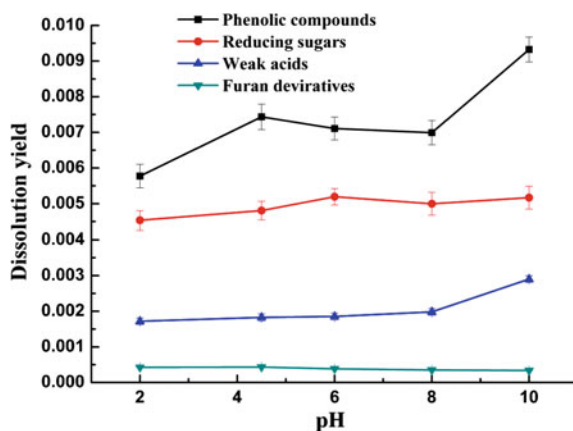
### 2.4.4 Effects of Ionic Strength on the Dissolution Rate of Degradation Products

As shown in Fig. 2.11, the effects of ionic strength on the dissolution of sugars, phenolic compounds, weak acids, and furfural derivatives are uniform; that is, the dissolution decreases with increased ionic strength.

**Fig. 2.11** Dissolution rate of degradation products of steam-exploded straw at different ionic strengths



**Fig. 2.12** Dissolution rate of degradation products of steam-exploded straw at different pH



#### 2.4.5 Effects of pH on the Dissolution Rate of Degradation Products

It can be seen from Fig. 2.12 that the dissolution yields of carbohydrate and weak acids increase with the increase of pH. Dissolution yields of carbohydrate reached the maximum at pH 6. For dissolution of weak acids, the larger the pH, the better the dissolution efficiency. Dissolution yields of furan derivatives are decreased with the increase of pH, which illustrates that the acidic condition is beneficial for dissolution yields of furan derivatives. From Fig. 2.12, dissolution yields of phenolic compounds are increased with the increase of pH at pH 2.0–4.5, but decreased with the increase of pH at pH 4.5–8.0. The dissolution rate in pH 10 is increased sharply. The reason maybe that lignin is degraded again in the dissolution process under alkaline conditions, which increases the content of phenolic compounds. Thus, from the point of dissolution and no damage of the original structure of the material, it should not be selected alkaline conditions to dissolve the degradation products, and dissolution rate of phenolic compounds reached the maximum at pH 4.5.

#### 2.4.6 Optimal Dissolution Conditions for Sugars and Phenolic Compounds

Steam explosion is used to enhance the enzymatic hydrolysis of lignocellulosic substrates into glucose and to produce hemicellulose hydrolysates with the highest yields of pentosan, which is a substrate for industrial fermentation. However, weak acids, furfural derivatives, and phenolic compounds in steam explosion hydrolysates are regarded as potential fermentation inhibitors that should be removed to reduce inhibition to strains before fermentation. Therefore, the separation of sugars

and potential fermentation inhibitors through dissolution eliminates the detoxification process for the fermentation industry and provides a reference for the recovery of sugars, which is beneficial to their subsequent self-conversion and utilization.

The tolerances of different strains to different types of inhibitors are inconsistent. Phenolic compounds and furfural derivatives are the most toxic to common microorganisms. The effects of dissolution conditions on furfural derivatives are not obvious. Thus, the dissolution of phenolic substances is used as the basic reference for dissolution inhibition. Results indicates that the optimal dissolution conditions for phenolic compounds are 100 °C (the higher, the better), LSR of 25, and ionic strength of 0.020 mol/L (the smaller, the better). The most unfavorable dissolution conditions are 20 °C (the lower, the better), LSR of 10, and ionic strength of 0.20 mol/L (the higher, the better). The optimal dissolution conditions for sugars are 20 °C, LSR of 20, and ionic strength of 0.02 mol/L (the smaller, the better). Thus, dissolution conditions can be controlled at 20 °C (or room temperature), LSR of 20, and ionic strength of 0.02 mol/L (the ionic strength is not deliberately adjusted because its value in natural waters is lower than 0.02 mol/L) to maximize the dissolution of sugars and minimize dissolution of phenolic substances.

### 2.4.7 Dissolution Thermodynamic Principles for Degradation Products in SE

Chemical potential and activity are associated with the diffusion and desorption of products in the dissolution process for SES degradation. These products can transfer from high-chemical potential and high-activity systems to ones.

Figure 2.13 shows that the dissolution process of SES degradation can be considered as a change of state from 1 to 2. The main parameters in the solution are  $\mu$ ,  $\alpha$ ,  $\gamma$ , and  $C$ .  $\mu$  is the chemical potential,  $\alpha$  is the activity,  $\gamma$  is the activity coefficient, and  $C$  is the theoretical concentration.

The dissolution process of SES degradation products include desorption and dissolution. Thus, the partial molar free energy change from state 1 to state 2 is  $\Delta G = \Delta G_1 + \Delta G_2$  (1 refers to desorption; 2 refers to dissolution). The material has

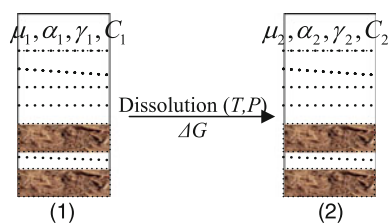


**Fig. 2.13** Dissolution process of degradation products of steam-exploded straw

not yet begun to dissolve in state 1. Thus, the parameters considered are the intrinsic parameters of the steam-exploded materials (the sugar concentration depends on the steam explosion pretreatment):  $C_1 = \Delta m / (m \times \chi_1)$  and  $C_2 = \Delta m / (m \times \chi_2)$ , where  $\Delta m$  is the reduction of hemicellulose or lignin in the materials,  $m$  is the mass of dry steam-exploded materials,  $\chi_1$  is the LSR for steam-exploded materials (in general, LSR is 0.5–0.7; in this equation, LSR = 0.6), and  $\chi_2$  is the LSR for the washing process.

In the desorption process,

$$\Delta G_1 = RT \ln \frac{C_2}{\alpha_2} = RT \ln \frac{1}{\gamma_2} \quad (2.64)$$

In the dissolution process,

$$\Delta G_2 = RT \ln \frac{C_2}{C_1} = RT \ln \frac{\chi_1}{\chi_2} = RT \ln \frac{0.6}{\chi_2} \quad (2.65)$$

Thus,

$$\Delta G = \Delta G_1 + \Delta G_2 = RT \ln \frac{0.6}{\gamma_2 \cdot \chi_2} \quad (2.66)$$

Therefore, the partial molar free energy change in the dissolution process of SES degradation products from state 1 to state 2 is given as follows:

$$\Delta G = RT \ln \frac{0.6}{\gamma_2 \cdot \chi_2} = -RT \ln K_a^\ominus + RT \ln Q_a = RT \ln \frac{K_a^\ominus}{Q_a} \quad (2.67)$$

where  $K_a^\ominus$  is the dissolution equilibrium constant and  $Q_a$  is the activity provider. At dissolution time  $t = 0$ , the concentration of the soluble molecules in the solution is zero. Thus,  $Q_a = 0$ . When dissolution reaches equilibrium,  $Q_a = K_a^\ominus$ . Therefore,  $\Delta G$  is a constant negative in the dissolution process, indicating that the dissolution of soluble molecules is spontaneous and accompanied by free steam explosion degradation.

According to Eq. (2.67), the factors affecting the dissolution process during water washing are the dissolution temperature  $T$ , activity coefficient  $\gamma_2$ , and LSR  $\chi_2$ . The activity coefficient of the nonelectrolyte liquid mixtures is related with van der Waals forces, hydrogen bonding, complex forces in electronic transfer, and so on [26]. According to the literature [27], the activity coefficient  $\gamma$  of the nonelectrolyte solute is inversely proportional to the electrolyte concentration. The electrolyte concentration can be regarded as the ionic concentration. Therefore, a smaller ionic strength results in a higher activity coefficient of the nonelectrolyte solute. Equation (2.67) shows that higher activity coefficient  $\gamma_2$  and LSR result in smaller free energy; a more negative  $\Delta G$  value indicates easier dissolution of steam explosion degradation products.



According to the van't Hoff equation,  $\frac{d\ln K^\ominus}{dT} = \frac{\Delta_r H^\ominus(T)}{RT^2}$ . Thus, the dissolution of phenolic compounds is endothermic, whereas the dissolution of sugar molecules is exothermic. Therefore, steam-exploded materials can be washed at room temperature. This process benefits sugar molecules dissolution but not phenolic molecules dissolution.

Fractionation of sugars and phenolic compounds during the process of dissolution eliminates the need for subsequent detoxification in the fermentation industry. These results provide a theoretical reference for the efficient dissolution of sugars and for overcoming the barrier to cellulose hydrolysis.

## 2.5 Formation Kinetics of Potential Fermentation Inhibitors in a Steam Explosion Process of Corn Straw

### 2.5.1 Overview

Lignocellulose, which is a complex of cellulose, hemicelluloses, and lignin, only renders approximately 20 % of its theoretical glucose yield upon subjection to enzymatic hydrolysis due to its recalcitrance [28]. Therefore, lignocellulose needs to be pretreated to enable the cellulose to be more accessible to cellulolytic enzymes [29].

Various researchers have demonstrated the capability to identify and/or quantify sugars and lignin degradation products resulting from chemical pretreatment of biomass. Fenske et al. [30] compared aromatic monomers in lignocellulosic biomass dilute acid prehydrolysates. Luo et al. [31] identified potential fermentation inhibitors in the conversion of hybrid poplar hydrolyzate to ethanol. Palmqvist et al. [32] discussed the generation of inhibitors during degradation of lignocellulosic materials by dilute acid pretreatment and reviewed the inhibiting mechanisms of individual compounds on fermentation yield and productivity. Klinke et al. [29] systematically summarized the different inhibitors formed by pretreatment of lignocellulosic materials and their inhibition of ethanol production in yeast and bacteria. Du et al. [33] researched the effects of varying pretreatment chemistry–feedstock combinations on degradation product formation and accumulation of biomass hydrolysates is analyzed. But the formation rules of potential inhibitors in steam explosion process are not reported in one consolidated study.

### 2.5.2 Determination of Potential Fermentation Inhibitors in Steam Explosion Hydrolysates

Table 2.7 shows the quantitative determination of the identified degradation compounds in the hydrolysates from the steam-exploded corn straw. The acetic, formic

Table 2.7 Conversion of inhibitor at different temperature and time in steam explosion pretreatment

Time	T (K)	Conversions (MC × 100,000)			4-hydroxybenzaldehyde	Vanillin	p-coumaric acid	Acetic acid	Formic acid	p-hydroxybenzoic acid	Ferulic acid
		HMF	F	Syringic acid							
2 min	283	0.00	0.00	0.00	1.10	0.00	13.93	94.85	188.73	–	0
	294	1.97	0.00	0.00	4.91	4.80	40.73	249.58	171.85	–	0
	310	5.05	0.00	2.10	11.54	13.57	94.21	354.24	205.13	–	0
	328	16.99	0.00	2.14	12.30	18.23	96.28	579.97	239.14	–	0
	351	38.89	1.65	2.44	12.93	30.62	105.59	582.54	310.11	–	0
	378	44.80	3.15	2.67	14.77	30.36	68.71	635.40	341.47	–	0
	410	95.70	8.17	2.98	16.15	30.71	50.75	773.88	367.07	–	0
	471	96.96	17.74	4.32	20.07	36.93	37.77	1092.19	557.04	–	52.22
5 min	283	0.00	0.00	0.00	1.10	0.00	13.93	94.85	188.73	–	0
	294	6.67	0.00	0.00	6.94	5.19	43.16	278.70	227.93	–	0
	310	14.61	0.00	2.10	11.75	13.75	95.27	426.75	277.77	–	0
	328	35.84	1.41	2.24	16.02	26.46	99.36	585.55	304.87	–	0
	351	44.32	2.21	2.48	17.07	25.05	62.25	630.32	337.17	–	0
	378	102.04	7.75	2.83	17.46	32.12	39.66	750.89	479.27	–	0
	410	116.23	27.98	3.06	19.05	26.33	28.28	1062.70	616.28	–	0
	471	118.06	37.71	4.61	22.16	29.03	22.05	1118.04	654.03	–	58.13
8 min	283	0.00	0.00	0.00	1.10	0.00	13.93	94.85	188.73	–	0
	294	11.82	1.43	1.91	10.30	13.77	91.42	392.58	283.79	–	0
	310	19.23	1.98	2.14	12.33	20.41	96.34	517.91	335.71	–	0
	328	38.01	2.31	2.44	17.17	29.03	107.13	594.46	394.90	–	0
	351	47.98	2.57	2.54	17.07	26.42	76.60	670.26	419.30	–	0
	378	108.38	12.50	2.86	16.33	26.76	54.90	954.90	509.12	–	0
	410	119.58	56.75	4.32	16.31	27.23	38.30	1388.85	823.13	–	37.73
	471	138.39	73.52	5.04	16.13	27.06	35.04	1430.98	845.66	–	35.26

“—” mean trace

acids, HMF, and furfural acids from the hemicellulose degradation of corn straw are the main compounds present in the hydrolysate, which accounts for 82–96 % of the total inhibitors. *p*-coumaric acid, vanillin, 4-hydroxybenzaldehyde, and syringic acid constitute a large fraction of the lignin-derived compounds in the hydrolysate, which accounted for 3–14 % of the total inhibitors. Both *p*-hydroxybenzoic and ferulic acids are in small quantities in the hydrolysate, the sum of which accounts for less than 3 % of the total inhibitors. Vanillic and 4-hydroxybenzoic acids are not detected in the hydrolysate of steam explosion pretreatment.

In general, it is observed that the types and concentrations of degradation products produced during pretreatment are more dependent upon the feedstock utilized than on the type of pretreatment chemistry employed. However, formation and accumulation of select compounds are dependent upon both feedstock and pretreatment chemistry [33]. From Tables 2.7 and 2.8, the types of inhibitors observed in corn straw hydrolysates during different pretreatment technologies are almost the same. The yield of inhibitor is differed in various pretreatments. The yield of the weak acids is the highest in the  $\text{NH}_3 \cdot \text{H}_2\text{O}$  pretreatment, whereas the yield of furan derivatives is the highest in the dilute acid pretreatment. A few differences exist between the phenolic compound yields in different pretreatments. Vanillic and 4-hydroxybenzoic acids were not detected in the steam explosion pretreatment, whereas *p*-coumaric acid is detected only in the steam explosion pretreatment and not in other pretreatments.

**Table 2.8** Inhibitor conversion observed in corn straw hydrolysates

	All pretreatments were carried out at 180 °C, for 8 min						
Weak acids	0.7 % $\text{H}_2\text{SO}_4$	0.07 % $\text{H}_2\text{SO}_4$	LHW	Wet oxidation	$\text{NH}_3$	Lime	Oxidative lime
Acetic acid	1700.0	830.0	340.0	580.0	1800.0	1200.0	1100.0
Formic acid	1200.0	760.0	550.0	790.0	2500.0	430.0	920.0
<i>Furan derivatives</i>							
5-Hydroxymethylfurfural (5-HMF)	440.0	110.0	23.0	28.0	8.9	23.0	38.0
Furfural	2200.0	260.0	80.0	65.0	4.0	15.0	32.0
<i>Phenolic compounds</i>							
Vanillic acid	33.0	15.0	26.0	43.0	32.0	33.0	51.0
4-hydroxybenzoic acid	0.3	0.3	0.6	0.7	0.7	0.5	0.9
Ferulic acid	66.0	26.0	22.0	10.0	42.0	66.0	7.6
4-hydroxybenzaldehyde	36.0	24.0	27.0	44.0	15.0	22.0	21.0
Vanillin	40.0	28.0	26.0	67.0	26.0	36.0	17.0
Syringic acid	20.0	15.0	18.0	21.7	15.4	17.0	14.0
<i>p</i> -coumaric acid	0.0	0.0	0.0	0.0	0.0	0.0	0.0

All dates were the yield of each compound multiplying by 100,000

### 2.5.3 Yields of Inhibitors at Different Steam Explosion Conditions

Figures 2.14, 2.15, and 2.16 show the yield of furan derivatives, weak acids, and phenolic compounds versus temperature and time during the steam explosion pretreatment.

Figures 2.14 and 2.15 show an increase in the yield of furan derivatives and weak acids with the increase of pretreatment temperature and time. The same trend is observed with syringic acid (Fig. 2.16). However, the 4-hydroxybenzaldehyde, vanillin, and *p*-coumaric acids show typical characteristics of continuous reaction ( $A \xrightarrow[k_2]{k_1} B \xrightarrow[k_2]{k_1} C$ , where *A* denotes original corn straw, *B* represents the objective inhibitor, *C* denotes secondary degradation products, and *k* indicates equilibrium constant). Their yield does not have a linear relationship with the pretreatment temperature *T* and time *t*. The yields of the objective inhibitors in these reactions are

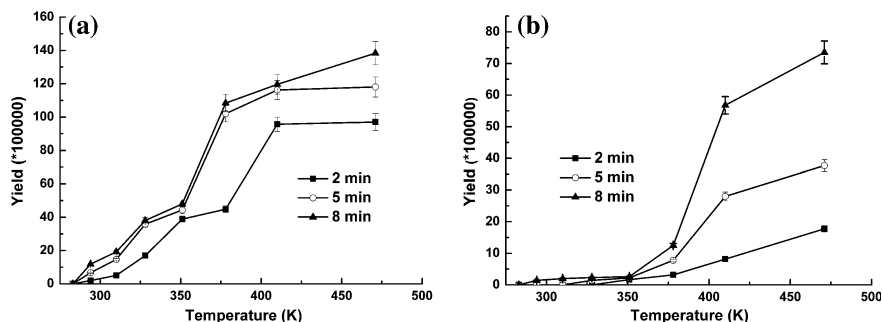


**Fig. 2.14** Effects of temperature and time of steam explosion on the yield of furan derivatives. **a** HMF. **b** Furfural

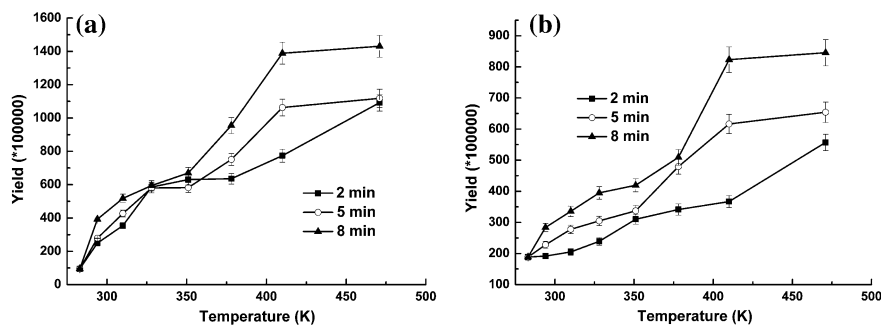


**Fig. 2.15** Effects of temperature and time of steam explosion on the yield of weak acid. **a** Acetic acid. **b** Formic acid

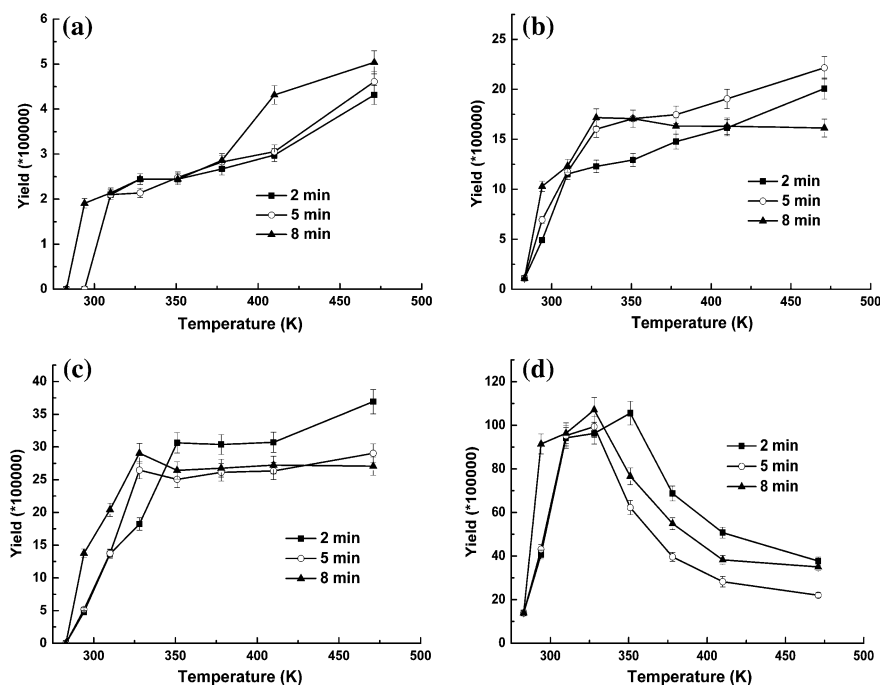


**Fig. 2.16** Effects of temperature and time of steam explosion on the yield of phenolic compounds. **a** Syringic acid. **b** 4-hydroxybenzaldehyde. **c** Vanillin. **d** *p*-coumaric acid

affected by  $k_1/k_2$  and time  $t$ . From the Arrhenius equation  $k = A \times e^{\frac{-E_a}{RT}}$ ,  $k$  is affected by  $E_a$  and  $T$ . Thus, the yields of the objective inhibitors are  $A_1 \times e^{\frac{-E_{a1}}{RT}} / A_2 \times e^{\frac{E_{a2}}{RT}} \cdot t$ , in which the extremum exists at a given  $T$  or  $t$ .

Sun and Chen (27) found that some lignin and carbohydrates form the lignin recondensation and/or LCC during the drying process of fiber. Under severe enough pretreatment conditions, the cleaved linkages of hemicellulose and lignin form other linkages, i.e., lignin recondensation (28–29). Formed lignin recondensation or LCC may be the reasons for the yield of 4-hydroxybenzaldehyde, vanillin, and *p*-coumaric acids not having a linear relationship with the pretreatment temperature  $T$  and time  $t$  but first increasing then dropping.

As shown in Fig. 2.16, when the pretreatment time  $t$  is less than 5 min, the yield of 4-hydroxybenzaldehyde increased with temperature. However, when  $t$  is 8 min, the yield initially increases and then decreases. It finally reaches the maximum at 328 K. At the same pretreatment time  $t$ , the yield of vanillin increases with temperatures from 283 to 351 K but remains unchanged at temperatures higher than

351 K. Moreover, when pretreatment time  $t$  is longer than 2 min and temperature is higher than 351 K, the yield of vanillin shows a downward trend. When pretreatment time  $t$  increases, the yield of  $p$ -coumaric acid increases with temperature increasing from 283 to 328 K. However, the yield of  $p$ -coumaric acid decreases at temperature beyond 328 K. The yield of  $p$ -coumaric acid at 5 min is larger than that at 8 min. This difference may be due to the larger  $k_1/k_2$  of  $p$ -coumaric acid at 8 min than that at 5 min.

### 2.5.4 Dynamic Parameters and Yield Equations of Inhibitors in Steam Explosion Process

Table 2.9 shows the equilibrium constants of the objective inhibitors at each temperature level. From Figs. 2.14, 2.15, and 2.16, the yield of HMF, furfural, syringic, acetic, and formic acids is positively correlated with pretreatment time and temperature. Thus, an equilibrium constant exists in each compound for each temperature level. The formations of 4-hydroxybenzaldehyde, vanillin, and  $p$ -coumaric acids are continuous reactions, and their yield is affected by several factors; thus, their equilibrium constants are difficult to express and not calculated here.

According to the equation  $\ln \kappa = \ln A - \frac{E_a}{RT}$ , the  $k$  versus  $1/T$  plot would yield an activation energy  $E_a$  and pre-exponential factor  $A$ . Tables 2.10 and 2.11 show the dynamic parameters and Arrhenius equations of the five model inhibitors, respectively.

Table 2.12 shows the yield equations of HMF, furfural, syringic, acetic, and formic acids. The yields of the inhibitors could be associated directly with the time and temperature of the steam explosion pretreatment. Thus, the yields of inhibitors could be predicted and calculated before the actual determination, even before the steam explosion experiment.

The analysis of the formation kinetics of eight kinds of fermentation inhibitors in the steam-exploded material hydrolysates shows that formations of weak acids and furan derivatives are the first-order reactions, of which conversions increase with the pretreatment temperature and time. Formations of phenolic compounds show typical characteristics of continuous reaction, of which conversions are affected by both active energies in two stages, temperature and time, and existed extreme value. Inhibitor conversion equations and relationships of inhibitor conversion, temperature, and time in steam explosion process are further deduced. Such understanding may contribute to predict and calculate the inhibitors conversions and to provide theoretical references for limiting the production of certain inhibitors by artificially controlling the temperature and holding time in steam explosion process.

**Table 2.9** Equilibrium constant of inhibitors in different temperatures

T(k)	Equilibrium constant $K \times \text{quilib}$									
	$A \xrightarrow[\tau]{\perp} kB$									
	HMF	Furfural	Syringic acid	Acetic acid	Formic acid	$A \xrightarrow[\tau]{\perp} [k_1 B \xrightarrow[\tau]{\perp} k_2 C]$	4-hydroxybenzaldehyde	Vanillin	$p$ -coumaric acid	
283	0	0	0	0	0		ND	ND	NE	
294	1.4175	0.1282	0.1716	54.121	40.362		NE	NE	NE	
310	2.5487	0.1782	0.3102	75.113	48.223		NE	NE	NE	
328	5.5625	0.2747	0.3767	95.090	55.503		NE	NE	NE	
351	7.3464	0.3756	0.4049	104.073	60.865		NE	NE	NE	
378	15.7729	1.560	0.4558	136.177	76.905		NE	NE	NE	
410	18.5933	6.5619	0.5995	193.248	111.833		NE	NE	NE	
471	20.3367	8.7330	0.7743	206.693	119.887		NE	NE	NE	

A original corn straw, B objective inhibitors, C secondary degradation products, NE not expressed

**Table 2.10** Pre-exponential factor and activation energy of five model inhibitors

	HMF	Furfural	Syringic acid	Acetic acid	Formic acid
Pre-exponential factor $A$	0.03248	0.2847	0.000072	0.02237	0.008671
Activation energy $E_a$	18080.51	30907.05	8509.953	8835.853	7504.466

**Table 2.11** Arrhenius equations of five model inhibitors

	Arrhenius equations
HMF	$K = 0.03248 \times e^{\frac{-2174.7}{T}}$
Furfural	$K = 0.2847 \times e^{\frac{-3717.47}{T}}$
Syringic acid	$K = 0.000072 \times e^{\frac{-1023.57}{T}}$
Acetic acid	$K = 0.02237 \times e^{\frac{-1062.8}{T}}$
Formic acid	$K = 0.008671 \times e^{\frac{-902.63}{T}}$

**Table 2.12** Yield equations of five model inhibitors

	Yield (Y) ( $T$ temperature, $K$ ; $t$ time, min)
HMF	$Y = 0.03248 \times e^{\frac{-2174.7}{T}} \times t$
Furfural	$Y = 0.2847 \times e^{\frac{-3717.47}{T}} \times t$
Syringic acid	$Y = 0.000072 \times e^{\frac{-1023.57}{T}} \times t$
Acetic acid	$Y = 0.02237 \times e^{\frac{-1062.8}{T}} \times t$
Formic acid	$Y = 0.008671 \times e^{\frac{-902.63}{T}} \times t$

## 2.6 Analysis of Energy Consumption on Steam Explosion Process

### 2.6.1 Overview

As an effective pretreatment method for biomass, although steam explosion technology is widely studied and applied [4, 5], most of existing research works only simply optimize the effect of holding pressure, holding time, and materials presoak treatment before steam explosion. Systematical research on heat transfer and energy consumption in steam explosion process is rare.

In view of this, the distribution of energy consumption in steam explosion process and their relationship are analyzed from heat transfer. Based on the actual steam explosion process, the effects of initial moisture content of materials, ratio of tank height to diameter, loading coefficient, and holding temperature on energy consumption are systematically investigated. The optimum condition where steam explosion energy consumption reaches the minimum value is obtained, and a retrieval table of steam explosion energy consumption at temperature of 143–212 °C (corresponding to the pressure of 0.4–2.0 MPa), holding time of 2–12 min, and



the initial moisture content of 20–80 % is calculated, which provides valuable guides for further economic analysis and material balance calculation in steam explosion related process.

### 2.6.2 The Composition of Steam Explosion Energy Consumption

Take industrial 20-m<sup>3</sup> tank as an example. Corn straw in temperature 20 °C will be heated to preset temperature by 220 °C inlet steam. Holding time is 5 min. As shown in Fig. 2.17, energy consumption in steam explosion process includes five parts: heating materials energy  $Q_1$ , heating the liquid water in materials energy  $Q_2$ , holding pressure energy  $Q_3$ , heating tank energy  $Q_4$ , and tank radiation energy  $Q_5$ .

### 2.6.3 Calculation Formulas for Each Part of Energy

Heating materials energy

$$Q_1 = c_1 m_1 \Delta t = c_1 m_{\text{total}} (1 - \omega) (T_1 - T_0) \quad (2.68)$$

Heating the liquid water in materials energy

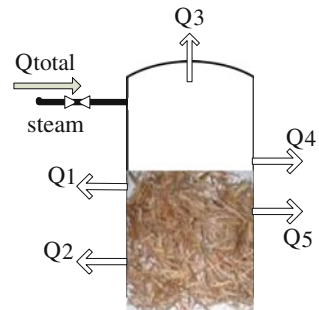
$$Q_2 = c_2 m_2 \Delta t = c_2 m_{\text{total}} \omega (T_1 - T_0) \quad (2.69)$$

Holding pressure energy

$$Q_3 = c_2 m_3 (T - T_1) + m_3 r \quad (2.70)$$

$$m_3 = \frac{PVM_w}{RT_1 \cdot 1000} \quad (2.71)$$

**Fig. 2.17** The distribution of steam explosion energy consumption



Tank radiation energy

$$Q_4 = \varepsilon \cdot c_0 \cdot \left( \frac{T_1}{100} \right)^4 \cdot A \cdot t \div 1000 \quad (2.72)$$

Heating tank energy

$$Q_5 = c_5 m_5 \Delta t = c_5 \cdot A \cdot \rho (T_1 - T_0) \quad (2.73)$$

Effective energy

$$Q_e = Q_1 + Q_2 + Q_3 \quad (2.74)$$

Ineffective energy

$$Q_{ine} = Q_4 + Q_5 \quad (2.75)$$

Total energy

$$Q_{total} = Q_1 + Q_2 + Q_3 + Q_4 + Q_5 \quad (2.76)$$

Steam consumption per unit mass dry basis

$$m' = \frac{Q_{total}}{m_{total}(1 - \omega)} \quad (2.77)$$

where  $c_1$  is specific heat capacity of materials. Because the material is corn straw, then  $c_1 = 1.6 \text{ kJ/kg K}^{-1}$  [34];

$m_1$  is the mass of dry material, kg;

$m_{total}$  is the mass of wet material, kg;

$m_2$  is the mass of water in wet material, kg;

$\omega$  is moisture content of wet material;

$T_1$  is holding temperature of the material, K;

$T_0$  is initial temperature of the material, K;

$c_2$  is specific heat capacity of liquid water, taking  $c_2 = 4.2 \text{ kJ/kg K}^{-1}$ ;

$m_3$  is steam consumption in holding pressure process, kg;

$T$  is inlet saturated steam temperature, K;

$r$  is condensing heat of saturated steam, kJ/kg;

$P$  is holding pressure, Pa;

$V$  is the volume of the tank,  $\text{m}^3$ ;

$M_w$  is molar mass of water;

$\varepsilon$  is blackness of stainless steel, taking  $\varepsilon = 0.60$  [35];

$c_0$  is blackbody radiation coefficient, taking  $c_0 = 5.67 \text{ W/(m}^2 \text{ K}^4)$ ;

$A$  is the surface area of the tank,  $\text{m}^2$ ;

$t$  is holding time, s;

**Table 2.13** Factor levels table on steam explosion energy consumption

Level of codes value	Ratio of height to diameter A	Charging coefficient B	Moisture of material C	Holding temperature D
2	5	100	0.9	212
1	4	80	0.7	197
0	3	60	0.5	182
-1	2	40	0.3	167
-2	1	20	0.1	152

$c_5$  is specific heat capacity of the tank material, and tank is made of stainless steel, then  $c_5 = 0.46 \text{ kJ/kg K}^{-1}$ ;  
 $m_5$  is the mass of the tank, kg;  
 $\rho$  is the density of stainless steel,  $\rho = 7.8 \text{ kg/m}^3$ .

## 2.6.4 Experiment Design and Data Processing

Select the ratio of tank height to diameter, loading coefficient, initial moisture content of materials, and holding temperature as four factors. Design factor levels as Table 2.13 and adopt quaternary cubic regression analysis. The index is steam consumption per unit mass dry basis (kg steam/kg dry basis). Using design-expert 7.1.6 software to analyze the results.

### 2.6.5 Relationship Between the Ratio of Tank Height to Diameter, Loading Coefficient, Initial Moisture Content of Materials, Holding Temperature, and Total Energy Consumption

#### 2.6.5.1 Regression Model Establishment and Significance Test

Using design-expert 7.1.6 software for multiple regression analysis based on calculation results, obtain regression model of steam consumption per unit mass of dry basis(kg steam/kg dry basis)  $Y$  on the ratio of tank height to diameter  $A$ , loading coefficient  $B$ , the initial moisture content of materials  $C$ , and holding temperature  $D$ .

$$y = 0.6596 - 0.1512B + 0.2203C + 0.1641D + 0.4883C^2 + 0.2656C^3 (R^2 = 0.961) \quad (2.78)$$

**Table 2.14** Analysis of variance for response surface reduced cubic model

Source	Sum of squares	df	Mean square	F value	p value prob > F
Model	25.00	5	5.00	117.08	<0.0001
B–B	0.55	1	0.55	12.84	0.0015
C–C	0.39	1	0.39	9.09	0.0060
D–D	0.65	1	0.65	15.14	0.0007
C2	6.87	1	6.87	160.83	<0.0001
C3	3.39	1	3.39	79.28	<0.0001
Residual	1.02	24	0.043		
Lack of fit	1.02	19	0.054		
Pure error	0.000	5	0.000		
Corresponding total	26.02	29			

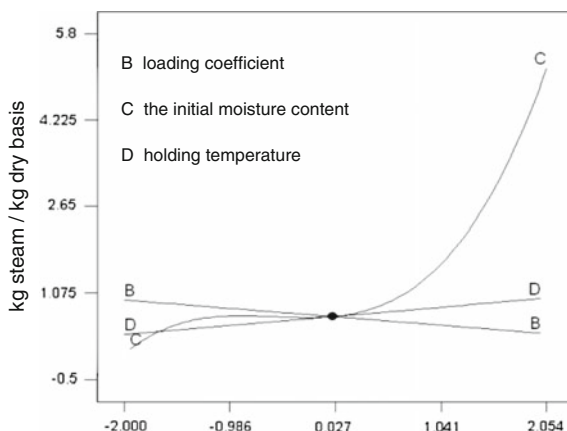
As shown in Table 2.14, the regression model  $p$  value is approximated to zero, significance level  $\alpha = 0.05$ ,  $P < \alpha$ ; then, it should reject the null hypothesis of regression equation significant test that the regression coefficient is not simultaneous as zero, and thus linear relationship between explanatory variables and independent variables is significant and linear model can be established. It also can be seen that the results of one degree term B, C, and D, quadratic term C2, and cubic term C3 all reach significant levels; then, using this model for analysis and forecasting steam consumption per unit mass of dry basis is reasonable. Coefficients of the standardization regression equation (2.78) reflect the effect of various factors on the index, and positive and negative coefficient reflects change direction of the index. It can be seen from one degree term of the four factors that the most influential factor on steam consumption per unit mass of dry basis is initial moisture content of materials, followed by holding temperature and loading coefficient, and the ratio of tank height to diameter has almost no effect on the index. Wherein the initial moisture content of materials and holding temperature both have positive impact on the index, loading coefficient has negative impact on it.

### 2.6.5.2 Single Factor Effect on Steam Consumption Per Unit Mass of Dry Basis (kg Steam/kg Dry Basis)

Other factors fixed at 0 level research the effect of one factor on steam consumption per unit mass of dry basis (kg steam/kg dry basis). Results are shown in Fig. 2.18.

As shown in Fig. 2.18, the change rate of initial moisture content of materials effect curve is maximum. When the code value of initial moisture content of materials is close to zero, the steam consumption per unit mass of dry basis is minimum (Theoretically, the code value of initial moisture content of material is the smaller the better, but it is difficult to achieve 10 % and below in actual situation, so the code value cannot be selected as -2). The larger loading coefficient lead to the

**Fig. 2.18** Single factor response curve to steam consumption per unit mass of dry basis (kg steam/kg dry basis)



smaller steam consumption per unit mass of dry basis, but the actual loading coefficient should be selected according to particle size and density of materials. With holding temperature decreasing, steam consumption per unit mass of dry basis would reduce, and choosing actual temperature should consider the requirements of pretreatment. The ratio of tank height to diameter has almost no effect on the index.

### 2.6.5.3 Determination the Optimal Conditions and Validation Regression Model

According to analysis results by design-expert 7.1.6 software, the best operating conditions include that the ratio of tank height to diameter is 3, loading coefficient is  $100 \text{ kg/m}^3$ , initial moisture content of materials is 0.44, and holding temperature is  $167^\circ\text{C}$ . Steam consumption per unit mass of dry basis is  $0.1948 \text{ kg steam/kg dry basis}$  under these conditions.

## 2.6.6 Energy Analysis of Steam Explosion Process

In steam explosion process, the energy consists of heating materials energy  $Q_1$ , heating the liquid water in materials energy  $Q_2$ , holding pressure energy  $Q_3$ , heating tank energy  $Q_4$ , and radiation energy of tank  $Q_5$ . Effective energy  $Q_e$  is defined as the sum of total heating energy of materials ( $Q_1 + Q_2$ ) with holding pressure energy  $Q_3$ . Ineffective energy  $Q_{ine}$  is defined as the sum of heating tank energy  $Q_4$  with radiation energy of tank  $Q_5$ . The ratio of each part of energy to total energy and the interrelation between each part of energy are seen as in the following analysis.

According to the formula,

$$\frac{Q_e}{Q_{ine}} = \frac{Q_1 + Q_2 + Q_3}{Q_4 + Q_5} = \frac{(T_1 - T_0)[c_1 m_{total}(1 - \omega) + c_2 m_{total} \omega] + [c_2(T - T_1) + r] \cdot \frac{PVM_w}{RT_1 \cdot 1000}}{\varepsilon c_0 \cdot \left(\frac{T_1}{100}\right)^4 \cdot A \cdot t + c_5 A \rho (T_1 - T_0)} \quad (2.79)$$

$$\frac{Q_e}{Q_{total}} = \frac{Q_1 + Q_2 + Q_3}{Q_1 + Q_2 + Q_3 + Q_4 + Q_5} = \frac{(T_1 - T_0)[c_1 m_{total}(1 - \omega) + c_2 m_{total} \omega] + [c_2(T - T_1) + r] \cdot \frac{PVM_w}{RT_1 \cdot 1000}}{(T_1 - T_0)[c_1 m_{total}(1 - \omega) + c_2 m_{total} \omega] + [c_2(T - T_1) + r] \cdot \frac{PVM_w}{RT_1 \cdot 1000} + \varepsilon c_0 \cdot \left(\frac{T_1}{100}\right)^4 \cdot A \cdot t + c_5 A \rho (T_1 - T_0)} \quad (2.80)$$

### 2.6.6.1 The Ratio of Each Part of Energy to Total Energy in Steam Explosion Process

Based on the above-optimized results, of which tank is 20 m<sup>3</sup>, the ratio of tank height to diameter is 3, loading coefficient is 100 kg/m<sup>3</sup>, initial moisture content of material is 0.44, and holding temperature is 167 °C. The results of ratios of each part of energy to total energy are shown in Fig. 2.19.

As shown in Fig. 2.19, the main energy are holding pressure energy (33.8 %), heating tank energy (27.3 %), and heating the liquid water in materials energy (23.9 %) in all compositions, and heating materials energy only accounts for 11.6 %. Tank radiation energy (3.3 %) can be negligible. Effective energy accounts for 70 % of the total energy, and ineffective energy is 30 %. According to the formulas (2.79) and (2.80), the ratio of effective energy to ineffective energy is mainly related to initial moisture content of materials and loading coefficient. It is inversely proportional to the ratio of tank height to diameter (mainly effect A) and has little relationship with holding temperature. On the optimized condition, of

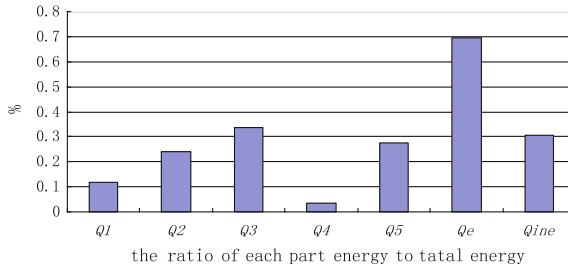


**Fig. 2.19** The ratio of five parts energy, effective energy, and ineffective energy to total energy. ( $Q_1$  heating materials energy,  $Q_2$  heating the liquid water in materials energy,  $Q_3$  holding pressure energy,  $Q_4$  heating tank energy,  $Q_5$  radiation energy of tank, effective energy  $Q_e = Q_1 + Q_2$ , and ineffective energy  $Q_{ine} = Q_4 + Q_5$ )

which the ratio of tank height to diameter is 3, loading coefficient is  $100 \text{ kg/m}^3$ , initial moisture content of materials is 0.44, and holding temperature is  $167^\circ\text{C}$ , and the ratio of effective energy to ineffective energy is 2.3 and the ratio of effective energy to total energy is 0.70. Thus, this result shows that the total energy mainly comes from the efficient energy, and effective energy mainly comes from the total heating materials energy. So the total energy can be optimized as long as we optimize the total heating materials energy. The total heating energy is only related to the initial moisture content of materials. That is, the initial moisture content of materials is the most important factor on total energy of steam explosion, which accords with the results of significant analysis and single factor analysis.

### 2.6.6.2 Relationship Between Each Part of Energy in Steam Explosion Process

According to the formula, the ratio of heating materials energy to heating the liquid water in materials energy is  $(1 - \omega)/\omega$ , which is only related to the initial moisture content of materials. From Fig. 2.20, the ratio of heating materials energy to heating the liquid water in materials energy reduces with moisture content increasing. That is, the proportion of heating straw decreases with moisture content increasing. Furthermore, it is known that the initial moisture content of materials cannot be too high; otherwise, most of the energy is used to heat the liquid water in materials, and this part of energy does not contribute to heating straw.

According to the formula  $\frac{Q_4}{Q_5} = \frac{\varepsilon \cdot c_0 \cdot \left(\frac{T_1}{100}\right)^4 \cdot t}{c_5 \cdot \rho \cdot (T_1 - T_0)}$ , the ratio of tank radiation energy to heating tank energy is related to the heating temperature based on the same holding time and the same volume of the tank. As shown in Fig. 2.21, the ratio of tank

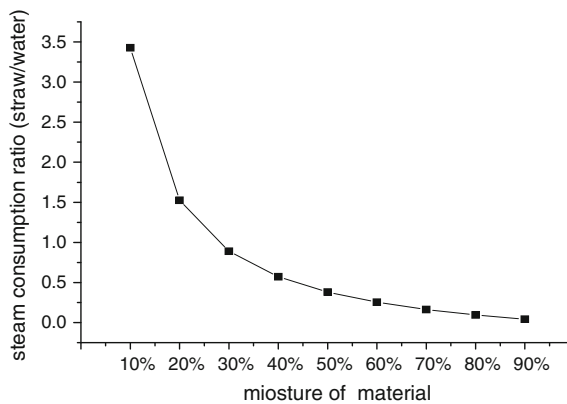
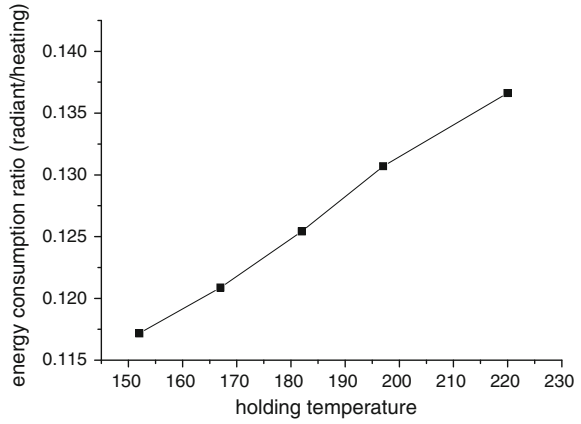


**Fig. 2.20** Effect of material moisture content on the ratio of heating materials energy to heating the liquid water in materials energy. Prerequisite:  $20\text{-m}^3$  tank, inlet steam temperature  $220^\circ\text{C}$ , heating the material from room temperature  $20\text{--}182^\circ\text{C}$ , and holding time 5 min

**Fig. 2.21** The ratio of tank radiation energy to heating tank energy on different holding temperature



radiation energy to heating tank energy is very small, and the maximum does not exceed 0.15. This implies that the tank radiation energy has little effect on the total energy. In addition, the equipment for industrial production and laboratory research all have insulation outside the tank, so the actual energy consumption is far lower than calculated value of radiation. Thus, the radiation energy loss is negligible. Because holding time only affects the tank radiation energy in all parts of energy, the effect of holding time on the overall energy consumption can be ignored since the radiation energy can be ignored. Steam explosion severity parameter formula [6]  $R_0 = t^{\exp(T-100)/14.75}$  ( $t$  is holding time, min;  $T$  is holding temperature, °C) shows that the strategy which holds low temperature and long time can be used to achieve the same steam explosion efficiency. Furthermore, based on the above analysis, holding low temperature is conducive to energy conservation. Thus, the strategy of holding low temperature and long time will not only ensure the same effect of steam explosion but also reduce energy consumption.

### 2.6.6.3 Building a Retrieval Table of Steam Explosion Energy Under Commonly Used Conditions

According to the formulas (2.68)–(2.77), calculate the steam consumption per unit mass of dry basis on the temperature conditions 143–212 °C (corresponding to the pressure 0.4–2.0 MPa), holding time 2–12 min, and the initial moisture content of materials 20–80 %. The results are shown in Table 2.15. Calculations are based on tank volume 20 m<sup>3</sup>, the ratio of tank height to diameter 3, and loading coefficient 100 kg/m<sup>3</sup>.

According to heat transfer, initial moisture content of materials is the most influential factor on total energy of steam explosion, and the best operating conditions are described as follows: the ratio of tank height to diameter is 3, loading coefficient is 100 kg/m<sup>3</sup>, initial moisture content of materials is 0.44, and holding



**Table 2.15** Steam consumption (kg steam/kg dry basis) under common conditions: temperature 143–212 °C (corresponding to the pressure 0.4–2.0 MPa), holding time 2–12 min, and the initial moisture content of materials 20–80 %

Y (kg steam/kg dry base)		t (min)						
T (°C)	ω (%)	2	4	5	6	8	10	12
143	20	0.207	0.208	0.209	0.209	0.211	0.212	0.213
	30	0.257	0.259	0.259	0.26	0.262	0.263	0.265
	40	0.324	0.326	0.327	0.328	0.33	0.332	0.333
	50	0.418	0.421	0.422	0.423	0.425	0.427	0.429
	60	0.56	0.562	0.564	0.565	0.568	0.571	0.573
	70	0.795	0.799	0.801	0.802	0.806	0.81	0.813
	80	1.266	1.271	1.274	1.277	1.282	1.288	1.293
152	20	0.234	0.235	0.227	0.237	0.239	0.241	0.243
	30	0.289	0.292	0.282	0.294	0.296	0.298	0.3
	40	0.364	0.366	0.355	0.369	0.371	0.374	0.376
	50	0.468	0.471	0.458	0.474	0.477	0.48	0.483
	60	0.624	0.628	0.612	0.632	0.636	0.639	0.643
	70	0.885	0.89	0.868	0.895	0.9	0.905	0.91
	80	1.406	1.414	1.381	1.421	1.429	1.436	1.444
164	20	0.253	0.255	0.255	0.256	0.258	0.26	0.261
	30	0.314	0.316	0.317	0.317	0.319	0.321	0.323
	40	0.395	0.397	0.398	0.399	0.401	0.403	0.406
	50	0.508	0.51	0.512	0.513	0.516	0.518	0.521
	60	0.678	0.681	0.683	0.684	0.688	0.691	0.694
	70	0.961	0.965	0.967	0.97	0.974	0.978	0.983
	80	1.527	1.533	1.537	1.54	1.547	1.553	1.56
175	20	0.279	0.28	0.281	0.282	0.284	0.286	0.288
	30	0.345	0.347	0.348	0.349	0.351	0.353	0.355
	40	0.433	0.435	0.437	0.438	0.44	0.443	0.445
	50	0.557	0.56	0.561	0.562	0.565	0.568	0.571
	60	0.742	0.746	0.748	0.749	0.753	0.757	0.76
	70	1.051	1.056	1.058	1.061	1.066	1.07	1.075
	80	1.668	1.676	1.68	1.683	1.691	1.698	1.705
180	20	0.296	0.298	0.299	0.3	0.302	0.304	0.306
	30	0.365	0.368	0.369	0.37	0.372	0.374	0.377
	40	0.458	0.461	0.462	0.463	0.466	0.468	0.471
	50	0.588	0.591	0.593	0.594	0.597	0.6	0.603
	60	0.783	0.786	0.788	0.79	0.794	0.798	0.802
	70	1.107	1.112	1.115	1.117	1.122	1.128	1.133
	80	1.756	1.764	1.767	1.771	1.779	1.787	1.795

(continued)

**Table 2.15** (continued)

Y (kg steam/kg dry base)		t (min)						
T (°C)	ω (%)	2	4	5	6	8	10	12
192	20	0.321	0.323	0.324	0.325	0.328	0.33	0.332
	30	0.396	0.399	0.4	0.401	0.404	0.406	0.409
	40	0.497	0.499	0.501	0.502	0.505	0.508	0.511
	50	0.637	0.64	0.642	0.644	0.647	0.651	0.654
	60	0.847	0.852	0.854	0.856	0.86	0.864	0.869
	70	1.198	1.204	1.207	1.209	1.215	1.221	1.227
	80	1.9	1.908	1.912	1.917	1.925	1.934	1.942
198	20	0.339	0.341	0.342	0.343	0.345	0.348	0.35
	30	0.417	0.42	0.421	0.422	0.425	0.428	0.43
	40	0.522	0.525	0.527	0.528	0.531	0.534	0.537
	50	0.669	0.673	0.674	0.676	0.68	0.683	0.687
	60	0.889	0.894	0.896	0.898	0.903	0.907	0.912
	70	1.256	1.262	1.265	1.268	1.274	1.28	1.286
	80	1.991	2	2.004	2.009	2.018	2.027	2.036
204	20	0.355	0.358	0.359	0.36	0.363	0.365	0.367
	30	0.438	0.44	0.442	0.443	0.446	0.448	0.451
	40	0.547	0.55	0.552	0.553	0.557	0.56	0.563
	50	0.7	0.704	0.706	0.708	0.712	0.715	0.719
	60	0.93	0.935	0.937	0.94	0.944	0.949	0.954
	70	1.313	1.32	1.323	1.326	1.332	1.339	1.345
	80	2.08	2.089	2.094	2.099	2.108	2.118	2.127
210	20	0.372	0.374	0.376	0.377	0.379	0.382	0.384
	30	0.457	0.46	0.462	0.463	0.466	0.469	0.472
	40	0.571	0.575	0.576	0.578	0.581	0.585	0.588
	50	0.731	0.735	0.737	0.739	0.743	0.747	0.751
	60	0.97	0.975	0.978	0.98	0.985	0.99	0.995
	70	1.369	1.376	1.379	1.382	1.389	1.396	1.402
	80	2.167	2.177	2.182	2.187	2.197	2.207	2.217
212	20	0.379	0.381	0.383	0.384	0.387	0.389	0.392
	30	0.466	0.469	0.47	0.472	0.474	0.477	0.48
	40	0.582	0.585	0.587	0.588	0.592	0.595	0.598
	50	0.744	0.748	0.75	0.752	0.756	0.76	0.764
	60	0.987	0.992	0.994	0.997	1.002	1.007	1.012
	70	1.392	1.399	1.402	1.405	1.412	1.419	1.426
	80	2.202	2.212	2.217	2.222	2.233	2.243	2.253

temperature is 167 °C. Steam consumption per unit mass of dry basis is 0.1948 kg steam/kg dry basis under these conditions. The proportion of the energy for heating straw is decreased with the increasing of moisture content. Thus, the initial moisture content of materials cannot be too high; otherwise, most of the energy is used to heat the liquid water in materials, and this part of energy does not contribute to heating straw. The effect of holding time on the overall energy consumption is negligible since the radiation energy can be ignored. Thus, the conditions of low holding temperature and long holding time will not only ensure the same efficiency of steam explosion but also reduce energy consumption. A retrieval table of steam explosion energy consumption under common conditions is established to provide a foundation for further economic analysis and material balance calculation.

## References

1. Chen HZ, Liu LY. Technology of steam explosion principles and application. Beijing: Chemical Industry Press; 2007.
2. Xie LS, Zhan HY. Pulping principle and engineering. Beijing: China Light Industry Press; 2001.
3. Yang SH. Plant fiber chemistry. Beijing: China Light Industry Press; 2001.
4. Alfani F, Gallifuoco A, Saporosi A. Comparison of SHF and SSF processes for the bioconversion of steam-exploded wheat straw. *J Ind Microbiol Biotechnol*. 2000;25(4): 184–92.
5. Datar R, Huang J, Maness PC. Hydrogen production from the fermentation of corn stover biomass pretreated with a steam-explosion process. *Int J Hydrogen Energy*. 2007;32(8):932–9.
6. Overend RP, Chornet E, Gascoigne JA. Fractionation of lignocellulosics by steam-aqueous pretreatments [and discussion]. *Phil Trans R Soc Lond A*. 1987;321(1561):523–36.
7. Helena L, Chum D, Stuart K. Organosolv pretreatment for enzymatic hydrolysis of poplars. 2. Catalyst effects and the combined severity parameter. *Ind Eng Chem Res*. 1990;29(2):156–62.
8. Belkacemi K, Abatzoglou N, Overend RP, Chornet E. Phenomenological kinetics of complex systems: mechanistic considerations in the solubilization of hemicelluloses following aqueous/steam treatments. *Ind Eng Chem Res*. 1991;30(11):2416–25.
9. Abatzoglou N, Chornet E, Belkacem K. Phenomenological kinetics complex systems: the development of a generalized severity parameter and its application to lignocellulosics fractionation. *Chem Eng Sci*. 1992;47(5):1109–22.
10. Montane D, Overend RP, Chornet E. Kinetic models for non-homogeneous complex systems with a time-dependent rate constant. *Can J Chem Eng*. 1998;76:58–68.
11. Hosseini SA, Shah N. Multiscale modelling of hydrothermal biomass pretreatment for chip size optimization. *Bioresour Technol*. 2009;100(9):2621–8.
12. Cantarella M, Cantarella L, Gallifuoco A. Comparison of different detoxification methods for steam-exploded poplar wood as a substrate for the bioproduction of ethanol in SHF and SSF. *Process Biochem*. 2004;39(11):1533–42.
13. Chen HZ, Chen JZ, Liu J, Li ZH. Studies on steam explosion of wheat straw I. Effects of the operating conditions for steam explosion of wheat straw and analysis of the process. *J Cellul Sci Technol*. 1999;7(2):60–7.
14. Chen HZ, Liu LY. Unpolluted fractionation of wheat straw by steam explosion and ethanol extraction. *Bioresour Technol*. 2007;98(3):666–76.
15. Cherepanov GP. Mechanics of brittle fracture. New York: McGraw-Hill; 1979.

16. Ning J, Wang C, Ma T. Explosion and shock dynamics. Beijing: National Defence Industry Press; 2010.
17. BenhamPP Warnock FV. Mechanics of solids and structures. Sweden: Pitman Publishing; 1973.
18. Wang X. Gas dynamics. Xi'an: Northwestern Polytechnical University Press; 2006.
19. Zhang YZ, Chen HZ. Multiscale modeling of biomass pretreatment for optimization of steam explosion conditions. *Chem Eng Sci*. 2012;75:177–82.
20. MosierN Wyman C, Dale B. Features of promising technologies for pretreatment of lignocellulosic biomass. *Bioresour Technol*. 2005;96(6):673–86.
21. Himmel ME, Ding SY, Johnson DK. Biomass recalcitrance: engineering plants and enzymes for biofuels production. *Science*. 2007;315(5813):804–7.
22. Selig MJ, Adney WS, Himmel ME. The impact of cell wall acetylation on corn stover hydrolysis by cellulolytic and xylanolytic enzymes. *Cellulose*. 2009;16(4):711–22.
23. Köhnke T. Adsorption of xylans on cellulosic fibres-Influence of xylan composition on adsorption characteristics and kraft pulp properties. Gothenburg: Chalmers University of Technology; 2010.
24. Ji XI, Huang H, Nie ZK. Fuels and chemicals from hemicellulose sugars. *Adv Biochem Eng Biotechnol*. 2012;128:199–224.
25. Chen YP, Yong Q, Liu CG, Xu Y, Yu SY. The microbes and selection of pentose fermentation. *J Cellul Sci Technol*. 2001;9(3):57–61.
26. Deng W, Shen B, Tang Y. The infinite dilution activity coefficient and selective molecules gravity. *J Hangzhou Normal University* 1991;(3): 55–59.
27. Bai T, Lu Y, Li Q. The infinite dilution activity coefficient of organic solutes in the mixture of formamide + salt. *J Henan Normal University*. 1996;24:48–51.
28. Chen HZ. Process engineering in plant-based products. Beijing: Chemical Industry Press; 2010.
29. Klink HB, Thomsen A, Ahring BK. Inhibition of ethanol-producing yeast and bacteria by degradation products produced during pre-treatment of biomass. *Appl Microbiol Biotechnol*. 2004;66(1):10–26.
30. Fenske J, Griffin D, Penner M. Comparison of aromatic monomers in lignocellulosic biomass prehydrolysates. *J Ind Microbiol Biotechnol*. 1998;20(6):364–8.
31. Luo C, Brink DL, Blanch HW. Identification of potential fermentation inhibitors in conversion of hybrid poplar hydrolyzate to ethanol. *Biomass Bioenerg*. 2002;22(2):125–38.
32. Palmqvist E, Hahn-Hägerdal B. Fermentation of lignocellulosic hydrolysates. II: inhibitors and mechanisms of inhibition. *Bioresour Technol*. 2000;74(1):25–33.
33. Du B, Sharma LN, Becker C. Effect of varying feedstock–pretreatment chemistry combinations on the formation and accumulation of potentially inhibitory degradation products in biomass hydrolysates. *Biotechnol Bioeng*. 2010;107(3):430–40.
34. He F, Du SS, Li YJ. Heat emission qualification of agro-stalks dring smoldering. *Biomass Chem Eng*. 2007;41(1):5–8.
35. TanT Dou M, Zhou M. Principles of chemical engineering. Beijing: Chemical Industry Press; 1984.

<http://www.springer.com/978-94-017-7412-3>

Gas Explosion Technology and Biomass Refinery

Chen, H.

2015, XIII, 364 p. 158 illus., 115 illus. in color.,

Hardcover

ISBN: 978-94-017-7412-3